Substrate dependent homeostatic control of c-di-AMP synthase (MsDisA) and hydrolase (MsPDE) from *Mycobacterium smegmatis*

Sudhanshu Gautam*[1], Avisek Mahapa*[1], Lahari Yeramala[2], Apoorv Gandhi[1], Sushma Krishnan[1], Kutti R. Vinothkumar[2], Dipankar Chatterji[#1]

[1] Molecular Biophysics Unit, Indian Institute of Science, Bangalore 560012, India, sudhanshu@iisc.ac.in (SG); avisek.mahapa@gmail.com (AM); apoorv.gandhi3@gmail.com (AG) and sushmak@iisc.ac.in (SM).

[2] National Center for Biological Sciences, Tata Institute of Fundamental Research, GKVK Post, Bellary Road, Bengaluru, India, ylahari@gmail.com (YL) and vkumar@ncbs.res.in (KRV)

* Equal contribution

Correspondence: dipankar@iisc.ac.in; Tel.: +91-80-2293-2836

Abstract

In bacteria, cyclic-di-nucleotide based second messengers regulate various physiological processes including the stress response. For the past few decades, cyclic diadenosine monophosphate (c-di-AMP) is emerging as a crucial second messenger in bacterial world. It is an essential molecule and has been implicated in fatty acid metabolism, antibiotic resistance, biofilm formation, virulence and activates the cytosolic pathway of innate immunity in host cell. The level of c-di-AMP is maintained within the cell by the action of two opposing enzymes, namely diadenylate cyclases and phosphodiesterases. However, such kind of c-di-AMP modulation remains to be explored in *Mycobacterium smegmatis.* Here, we systematically investigate the c-di-AMP synthase (MsDisA) and a hydrolase (MsPDE) from *M. smegmatis* at different pHs and osmolytic conditions. Our biochemical assays showed that the MsDisA activity is enhanced during the alkaline stress and c-di-AMP is readily produced without any intermediates. At pH 9.4, the MsDisA promoter activity increases significantly, further strengthening this observation. However, under physiological conditions, the activity of MsDisA is moderate with the formation of intermediates. We also observe that the size of MsDisA is significantly increased upon incubation with substrate. To further get deep insights into the structural characteristics, we report a 3.8 Å cryo-EM structure of the MsDisA protein, distinct from the earlier reported structure of DisA from *Thermotoga maritima.* The domain mutant experiments prove that the N-terminal minimal region can form a functional octamer. Thus, our

results reveal how mycobacterial c-di-AMP is biochemically and structurally regulated in response to different environment.

Keywords: *Mycobacteria*, second messengers, stress response, Cyclic-di-AMP, MsDisA, MsPDE, Cryo-EM

Introduction

All living organisms sense and process altered environmental stimuli through a cascade of complex signaling pathways. The bacterial signal transduction pathway is coordinated by secondary messengers during changes in temperature, nutrient concentration, pH, etc. Signaling nucleotide molecules so far include cyclic AMP, cyclic GMP, cyclic di-GMP, cyclic di-AMP, cyclic GAMP (cGAMP), and non-cyclic pGpp or (p)ppGpp. These nucleotide molecules interact with proteins or riboswitches to control cellular physiology (1-11). Among the second messengers, the regulatory network for c-di-GMP and (p)ppGpp signaling has been widely studied in bacteria. They appear to be global regulators of bacterial lifestyle. In bacteria, c-di-GMP mainly coordinates transition from a motile to a sessile state (8). It is also known to regulate biofilm formation, motility, virulence, cell cycle, antibiotic resistance, starvation, and many more pathways (8). The (p)ppGpp molecule mainly targets the transcription process to regulate cellular physiology (6). It is associated with bacterial survival under amino acid starvation, biofilm formation, cell cycle, virulence, etc. However, unlike c-di-GMP or (p)ppGpp, the regulatory pathway of c-di-AMP and cGAMP have not been extensively investigated yet. Only a few regulatory pathways governed by the c-di-AMP molecule have been reported earlier (2,12). The other second messenger, cGAMP, operates chemotaxis, virulence, and exoelectrogenesis in bacteria (4).

Cyclic-di-AMP was first identified during a structural investigation of the bacterial DNA integrity scanning protein (DisA) from *Thermotoga maritima* (13). Since its discovery, the molecule has been linked to crucial signaling processes like osmoregulation, DNA integrity maintenance, sporulation, cell-wall homeostasis, cell-wall biosynthesis, ion-channel homeostasis, antibiotic resistance, virulence gene expression, acid resistance, and carbon metabolism (2,14-16). In mycobacteria, c-di-AMP regulates fatty acid synthesis and DNA repair (17). Bacterial c-di-AMP secretion into the host cytosol has been reported in intracellular pathogens like *Listeria*

monocytogenes and *Mycobacterium tuberculosis* (18,19). It is known to trigger the formation of inflammatory molecules within the host cell during infection (10,20-24).

Cyclic-di-AMP is synthesized from two molecules of ATP by a **d**i-**a**denylate **c**yclase (DAC) domain-containing protein. A phosphodiesterase (PDE) can hydrolyze c-di-AMP into pApA or two molecules of AMP. In bacteria, a total of five classes of DAC domain-containing proteins (DisA, CdaA, CdaS, CdaM, and CdaZ) have been reported (3,25). DisA is a bi-functional octameric protein that can bind to the Holliday junction DNA or produce the c-di-AMP molecule (13). DisA primarily carries three domains (13). The N-terminal DAC domain is connected to the C-terminal DNA binding domain by a specific linker domain (Domain-2). The DAC domain interface (formed by the N-terminal interaction) is presumed to be the catalytic domain (13), and the synthesis of the c-di-AMP is dependent on the metal ions such as Mg^{2+} and Mn^{2+}. Cellular homeostasis of the c-di-AMP is modulated by a specific phosphodiesterase (PDE) located in a different operon that contains DHH-DHHA1 or HD (His-Asp) domain (26-28). The specific PDE can hydrolyze c-di-AMP into pApA or AMP. So far, the reported PDEs show a unique structural alignment (28). They consist of a signaling N-terminal linked to a degenerate GGDEF domain and a C-terminal DHH-DHHA1 module. This C-terminal DHH-DHHA1 domain is essential for the c-di-AMP hydrolysis. In *M. tuberculosis*, the PDE (also called CnpB) carries a core DHH-DHHA1 domain that hydrolyzes c-di-AMP in a two-step process: first to linear 5'-pApA, then hydrolyzed into two 5'-AMP molecules (27). *M. smegmatis* PDE (MSMEG_2630) also carries a DHH-DHHA1 domain and lacks other regulatory domains(26), which are conserved in the GdpP protein family (in *B. subtilis*). All types of PDEs require specific divalent metal ions (Mg^{2+}, Mn^{2+}, Co^{2+}) for their activity.

A few *disA* and *pde* phenotypes has been reported previously (12,14). In Gram-positive bacteria such as *S. aureus*, *B. subtilis* and *L. monocytogens*, c-di-AMP is essential for growth and showed lethal phenotype under standard growth conditions (12,14,29). On the contrary, the deletion of the *disA* gene in *M. smegmatis* barely affected bacterial survival but negatively influenced bacterial C_{12}-C_{20} fatty acids production. Whereas, MsPDE deletion mutant showed higher accumulation of intracellular C_{12}-C_{20} fatty acids (26). It is also reported that a deletion in PDE from *M. tuberculosis* showed less virulence in the infection model (30). The *radA* gene in *M. smegmatis* is present in the same operon as *disA*. It was reported earlier that RadA protein physically interacts with the DisA and negatively modulates c-di-AMP synthesis (25).

Because of the significance of c-di-AMP homeostasis in bacteria, we characterized c-di-AMP synthase MsDisA (MSMEG_6080) and hydrolase MsPDE (MSMEG_2630) from *M. smegmatis mc^{2}155* (3,26) at different pH and salt concentrations. Our enzyme kinetics and promoter assay data revealed that MsDisA is highly active at alkaline pH, and it quickly converts 2 molecules of ATP to c-di-AMP without forming any intermediates, whereas at neutral pH, MsDisA activity is reduced, and c-di-AMP is produced via intermediates, ppApA and pApA. We also found that c-di-AMP synthesis by MsDisA was inhibited by increasing concentration of ATP and the kinetics followed the substrate induced allosteric inhibition model. In case of MsPDE, hydrolysis of c-di-AMP at alkaline pH was slow with the formation of intermediates whereas at neutral pH, it hydrolyses c-di-AMP quickly with no intermediate formation. Biophysical characterization and Transmission Electron Microscopy (TEM) image analysis revealed the substrate induced modification of the MsDisA structure. We reconstructed a 3.8 Å structure of MsDisA by Electron Cryomicroscopy (Cryo-EM) and observed an open-complex formation of this protein. Our domain mutational studies revealed the minimal region required for the activity and oligomerization of MsDisA protein. This report attributes an additional function to c-di-AMP in regulating the alkaline stress response and gives new insights into c-di-AMP homeostasis contributed by DisA and PDE in *M. smegmatis.*

Results

Biochemical and functional characterization of MsDisA and MsPDE proteins

Initially, *disA* and *pde* genes from *M. smegmatis mc*^{2}155 were cloned in the pET28a vector and expressed in *E. coli* BL21(DE3). The recombinant MsDisA and MsPDE proteins were purified to homogeneity by affinity chromatography and analyzed by 10% SDS-PAGE (**Fig. S1, A and B**). The monomeric theoretical molecular mass of MsDisA and MsPDE are 40.51 kDa and 35.53 kDa, respectively. SDS-PAGE analysis revealed that the purified His-tagged proteins had the molecular weight mass of ~40 kDa and ~37kDa, respectively as expected. The identity of the pure proteins were confirmed by peptide mass fingerprinting (PMF) analysis (data not shown), and the molecular weight were found to be 41.3 kDa and 36.4kDa for MsDisA and MsPDE (with Hexahistidine-tag), respectively.

The oligomeric assemblies of the MsDisA and MsPDE proteins were studied by SEC-MALS. Our experimental data showed that the molecular mass of MsDisA and MsPDE proteins

were 334.5 kDa and 73.8 kDa, respectively (**Fig. 1A and B**). The determined molecular mass by SEC-MALS analysis indicates an octameric and dimeric assembly of the MsDisA and MsPDE proteins. The octameric and dimeric state of MsDisA and MsPDE is also supported by Transmission electron microscopy (TEM) analysis, which is discussed later.

Next, we checked the function of recombinant MsDisA and MsPDE for c-di-AMP synthesis and hydrolysis using HPLC analysis. The detector of HPLC was set at 254 nm to analyze the nucleotide products. For the synthesis activity, we have used both ATP and ADP as substrates (31,32). PDEs, on the other hand, would convert c-di-AMP to pApA or AMP. Few evidences suggest that they are nonspecific (26,27). PDE from mycobacteria hydrolyses both c-di-AMP and c-di-GMP (26).

As a control, commercial AMP, ATP, c-di-AMP were eluted from HPLC at 12.2, 17.4 and 23.7 mins, respectively **(Fig. 1C and D)**. Buffer from various pH and salt were used here. In a reaction catalyzed by MsDisA with ATP at pH 7.5 for 4h, two peaks were eluted at 20.3 min and 23.7 min **(Fig. 1E)**. However, the same reaction at pH 9.4 eluted a single peak at 23.7 min (**Fig. 1F**). The peak at 23.7 min was due to the formation of c-di-AMP as analyzed by the elution of pure nucleotide standard and subsequent LC-MS analysis (**Fig. S1, C**). The hydrolysis reaction was carried out at two pHs' 7.5 and 9.4 for 10min. C-di-AMP hydrolysis at pH 9.4 eluted two peaks at 12.2 min and 20.3 min (**Fig. 1G**), whereas c-di-AMP hydrolysis at pH 7.5 showed only one peak at 12.2 min (**Fig. 1H**). Hydrolysis reactions were comparatively faster and goes to completion at neutral pH 7.5. The peak at 12.2 min was found to be AMP.

The theoretical molecular mass of c-di-AMP, pApA and AMP are 658.4 Da, 676.4 Da, and 347.2 Da, respectively. Our reaction product resulted in the same molecular mass in both MsDisA and MsPDE reactions within error limits. Further confirmation came from MS-MS analysis of the products and validation with the standards (**Fig. S1, D and E**).

The peak eluting at 20.3 min in both the synthesis and hydrolysis reaction depended on the reaction condition and will be discussed later. The molecular masses of the eluates from synthetic reaction were 677.1 $[M+H]^+$ and 755 $[M-H]^-$, which are same as pApA and ppApA, respectively (Fig. S1, F). As MsDisA did not show any hydrolysis activity, we inferred that they are formed as synthetic intermediates (31,32). On the other hand, MsPDE only yielded an

intermediate at 677.1 $[M+H]^+$, probably due to pApA (**Fig. S1, D**). We propose here that the synthesis of the c-di-AMP goes through intermediates pApA and ppApA, whereas the hydrolysis of the c-di-AMP takes place via pApA. However, we were unable to resolve the peak at 20.3min to pApA and ppApA.

Maximum activity of MsDisA at alkaline pH and MsPDE at neutral pH

Proteins are evolved to perform a precise function in a specific physiological condition. A suitable buffer condition always plays a significant role in maintaining a particular protein's stability, function, structure, and oligomerization (33).

In vivo homeostasis of the c-di-AMP is linked to different conditions like osmotic pressure, pH, antibiotics, etc (1-3). While performing the activity analysis of MsDisA and MsPDE, we observed that the c-di-AMP synthesis and hydrolysis rate were altered upon changing the buffer conditions (pH and salt of the buffer). We also observed that the formation and hydrolysis of c-di-AMP took place via intermediates depending on the pH of the media. Thus, we checked further the *in vitro* activities of MsDisA and MsPDE at different pH (5.4, 7.5 and 9.4) and salt (75mM – 500mM). The reaction was followed by reverse-phase HPLC. The area under curve (AUC) for each peak was taken to measure the product formation. It can be seen from **Fig. 2** that in 4hrs, maximum activity for MsDisA was observed at pH 9.4 and NaCl concentration of 75mM. A significant decrease in activity can be seen in other pHs and salt (**Fig. 2A and B**).

Additionally, we noticed here that at pH 7.5, the c-di-AMP synthesis is accompanied by the formation of stable intermediates. When we performed the activity assay for MsPDE under similar conditions as that of MsDisA, we observed that the hydrolysis of the c-di-AMP is more efficient at pH 7.5, at 75mM NaCl (**Fig. 2C and D**). In this case too, the marginal formation of intermediates were noticed. From the above results, we depict the reaction pathway as shown in **Fig. 2G.** We believe this scheme is intrinsically connected to the participation of different substrates at the enzyme's active site and will be discussed in a later section.

MsDisA and MsPDE activity are modulated by higher substrate concentration.

The c-di-AMP molecule is known as an 'essential poison' as this molecule is indispensable for bacterial survival in stressed cells and reported to be toxic when over-accumulated in cells (28). So, the synthesis and hydrolysis of this molecule should be maintained

at equilibrium to sustain healthy cellular physiology. Here, we have performed steady-state kinetic experiments to follow the rate of making and breaking of the c-di-AMP molecule by MsDisA and MsPDE proteins. To quantitate the product formation, we followed the HPLC-based quantification method with a standard protocol. A standard curve of the c-di-AMP/ATP/AMP (µM) was prepared from the AUC values of the HPLC peak at different nucleotides concentrations (µM) (data not shown).

The activity assays for the MsDisA and MsPDE proteins were performed at different pH with 75mM NaCl. To calculate the kinetic parameters of MsDisA, we plotted the variation in rate of formation of the c-di-AMP at varying substrate concentrations. However, our data could not be fit well with standard Michaelis–Menten analysis or Lineweaver–max Burk plot. But the kinetic data follows a substrate inhibition model following the equation as shown in the material and method section (equation 1) with an R^2 value of 0.95. Different kinetic parameters like V_{max}, K_m and K_i values were obtained from the equation and reported in Tables 1 and 2. The in *vitro* MsDisA activity is inhibited by higher ATP concentrations (K_i> 2.8 µM) at pH 9.4. It appears that the cellular ATP pool regulates MsDisA enzyme activity. Analysis of the kinetic data revealed that at pH 5.4 and 7.5, the MsDisA protein also follows the substrate inhibition model, and the results are shown in **Fig. 2E**. However, the c-di-AMP synthesis rate at pH 5.4 and 7.5 is prolonged than that at pH 9.4. Interestingly, the same substrate inhibition model is followed by MsPDE at pH 9.4 (**Fig. 2F**). The kinetic parameters are reported in Table-1 and 2.

MsDisA promoter is responsive to alkaline stress

To determine the factors that affect c-di-AMP homeostasis *in vivo*, we cloned the putative MsDisA and MsPDE promoter regions into a promoter-less eGFP expression vector (**Fig. 3A and B**). The constructs containing the putative promoter regions of MsDisA and MsPDE were transformed into *M. smegmatis mc*^{2} 155 cells. Mycobacterial cells were then exposed to different stress conditions like alkaline and osmotic stress to study the promoter activity. Here we measured and correlated the eGFP expression level as protein synthesis under a specific physiological stress condition. In addition, the amount of protein synthesized was directly linked to the c-di-AMP homeostasis in the cell.

We observed that the MsDisA promoter activity was significantly increased at pH 9.4 compared to that of at pH 7.5 after 60h and 70h of growth, which matches with *in vitro* data (**Fig.**

3C). In comparison, the MsPDE promoter activity remained unchanged under alkaline stress throughout mycobacterial growth (**Fig. 3C)**. The higher production of the c-di-AMP was associated with osmotic stress and has been reported in many studies (1,16,34). As a control, we grew mycobacteria under osmotic stress, where cells were exposed to 0.5M KCl/NaCl stress and the promoter activity was measured after 60h and 70h of growth. As expected, we noticed higher promoter activity in the 0.5M KCl/NaCl containing media. Surprisingly, we also noticed higher promoter activity in the glucose starved cells (**data not shown**). No variation in the Hsp60 promoter activity under similar stress was noticed, which acted as a positive control.

Change in the conformation of MsDisA in the presence of ATP

Protein flexibility is one of the critical parameters for protein activity. In an enzyme-substrate reaction, domain movement in enzyme is often accompanied by substrate binding. To enumerate the substrate-induced structural changes for the c-di-AMP synthase and hydrolase, we recorded microscale thermophoresis (MST), far-UV CD spectra and TEM images of MsDisA and MsPDE proteins with or without substrate (ATP or c-di-AMP). The estimation of the binding affinity of the ATP to MsDisA at varying pH (5.4, 7.5 and 9.4) was carried out using MST and Kds' were obtained (Table 3), suggesting maximum ATP binding at pH 7.5 (**Fig. 4A-C)**. Our biophysical characterization suggested that MsDisA and MsPDE proteins are predominantly α-helical (**Fig. 4D and E)**. An exciting observation was made when we recorded far-UV CD spectra of MsDisA at pH 7.5 along with ATP, 222nm minima shifted to 208nm which clearly showed ATP-induced structural alteration in the MsDisA+ATP complex (**Fig. 4D**). To find out the specificity of the interaction, we also recorded the CD spectra of MsDisA with GTP, which revealed no changes in the far-UV CD spectra (data not shown). We also measured far-UV CD spectra of MsPDE with c-di-AMP (**Fig. 4E)** and found no change in helicity.

Substrate-induced structural alteration was also mapped by TEM image analysis of the MsDisA and MsDisA+ATP complex at pH 7.5. The TEM analysis of MsDisA reveals a higher order assembly, which is an octameric state corroborating with SEC-MALS data **(Fig. 4F).** To visualize the substrate-induced structural changes in MsDisA, we have collected the TEM images of the MsDisA (Fig. **S2, A**) and MsDisA+ATP (Fig. S2, B) complex and measured the length and width of the protein (**Fig. 4F and G**). We noticed that the average length and width of the MsDisA protein was 17.58±1.07nm and 7.3±0.7 nm (N=1050), respectively. However, upon

ATP complexation, the length and width of the MsDisA+ATP complex were significantly increased to 19.73±0.95 nm and 8.3±0.8nm (N=1100), respectively. In case of MsPDE, we did not notice any changes in c-di-AMP bound protein in comparison to that of MsPDE alone (Fig. **S2, C and D**).

Cryo-EM structures of the MsDisA: An open complex

To better understand the structure of MsDisA and the arrangement of the subunits, we performed single particle cryo-EM on purified protein. 720 images were collected on holey carbon grid coated with thin carbon layer and processed with software Relion 3 (35) and cryoSPARC (36). Best 2D classes were used to generate three initial models in cryoSPARC with no symmetry imposed (**Fig. S3, A**). In all three maps, we observed the opening at the active site in MsDisA maps in comparison to closed map of DisA with D4 symmetry from *Thermotoga maritima* as published in the crystal structure (PDB-3C1Z). We merged the two maps with similar densities and obtained a 3D reconstruction after non-uniform refinement to an overall resolution of 3.8 Å (**Fig. S3, B**), which clearly reveals distinct monomers (**Fig. 5A-C**). The local resolution plot shows that the core (DAC domain) resolved between 3.1-4.5 Å with lower resolution at the periphery (**Fig. S3, C**). The model of MsDisA was generated using either SWISS-MODEL (37) or the AlphaFold model of *M.tuberculosis* DisA as template (38). The secondary structure was used for docking the monomer into the cryoEM map and the model was manullay inspected and corrected (**Fig. 5A and B**). The C-terminus of the enzyme show larger flexibility and the maps of some monomer are better ordered than the others. The splayed apart C-terminus of MsDisA possibly reflects a open complex. For instance, monomer C (Teal ocean) and E (orange) are away by ~20 Å and this movement might be important for the catalytic activity. This open form is distinct from the crystal structure of the TmDisA, where all the monomers are equal (**Fig. 5C-F**).

N-terminal domain of MsDisA is sufficient for c-di-AMP synthesis and octamerization

The DisA protein consists of three structural domains; a nucleotide-binding domain (domain-1) and a DNA binding domain (domain-3). The N-terminal nucleotide-binding domain is attached to the C-terminal DNA binding domain via a helical linker domain-2 (13). Due to limitations on the resolution of the cryoEM map (particularly the C-terminal regions), we then

pursued biochemical approach to study each domain separately to follow the domain inter-dependency and structural integrity of the MsDisA. Based on the MsDisA cryo-EM map (**Fig. 5C**), different deletion mutants were isolated and characterized, as shown in the model (**Fig. 6A).** Each of these proteins were tested for c-di-AMP synthesis, TEM analysis, and their oligomerization status by SEC-MALS. It can be seen from **Fig. 6B** that $MsDisA_{1-316}$ forms oligomeric assembly and synthesizes c-di-AMP (**Fig. 6C and D**). The mutant $MsDisA_{1-158}$ also assembled as an oligomer of 8-subunit and synthesized c-di-AMP like wild-type protein (**Fig. 6E, F and G**). The mutant $MsDisA_{132-372}$ was found to be a dimer from SEC-MALS experiment (**Fig. 6H**), but we failed to detect the same by TEM analysis. The N-terminal deleted mutant also did not show catalytic activity (**Fig. 6I**). We propose that mutant $MsDisA_{132-372}$ is insufficient to maintain the higher order symmetry due to the absence of the N-terminal domain. This oligomerization pattern in the domain mutants confirmed that the octameric assembly of the MsDisA protein occurs through N-N terminal interaction.

Our next approach was to analyze the substrate (ATP) interaction with the active site of the MsDisA protein. For this purpose, we took the molecular docking analysis by Schrödinger (39) using MsDisA model and followed ATP/c-di-AMP interaction at the active site (**Fig. 6J and K**). It can be seen from Fig. 6J and K that, Asp84, Gln102, Leu103, Val104, Thr116, Arg117 and H118 are crucial for ATP binding and the residues Asp84, Gly 115, Thr 116, Arg117, His137 are essential for the c-di-AMP release. Based on the analysis, we created point mutations at the 84th, 102nd, 103rd, 118th and 137th positions of the MsDisA. These mutant proteins of MsDisA D84A, D84E and H137A were inactive as they could not synthesize c-di-AMP (**Fig. S4, A-D**). In the MsDisA H118A, we detected a small amount of c-di-AMP synthesis in the reaction suggesting that H118 is crucial for the activity (**Fig. S4, E**).

Discussion

As a multi-function molecule, c-di-AMP has been implicated in potassium transport, osmotic stress, acid stress, cold stress, DNA repair, sporulation, drug resistance, genetic competence, central metabolism, day-night cycle in cyanobacteria, fatty acid biosynthesis and biofilm formation (26,40-48). Apart from facilitating bacterial adaptation to various environmental stresses, it can influence the virulence of several pathogenic bacteria (14) and the host immune responses (18,49). These functions are mediated via c-di-AMP binding to the

multitude of receptors housed in different protein families and riboswitches as a crucial alarmone in bacteria and archaea (12). Inadequate or excessive concentrations of c-di-AMP affect bacterial growth in both normal and abnormal circumstances. Therefore, sustaining the optimum concentration of c-di-AMP is important in bacteria and it is achieved by the two key players, DACs and PDEs.

In this work, we report the homeostasis of c-di-AMP by DisA and PDE in *M. smegmatis* and the substrate induced inhibitory mechanism of MsDisA. For this purpose, we have purified a c-di-AMP synthase (MsDisA) and hydrolase (MsPDE) to homogeneity from *M. smegmatis* $mc^2$155. Enzyme assays and the mass spectrometry analysis of the assay products confirmed the presence of c-di-AMP and AMP as final products in the MsDisA synthesis and MsPDE hydrolysis reactions, respectively. MsDisA from *M. smegmatis* is an ortholog to the *M. tuberculosis* Rv3586 (DacA) and *B. subtilis* DisA, putative di-adenylate cyclases. It has been reported earlier that the c-di-AMP formation in *M. tuberculosis* Rv3586 (MtbDac) is a two-step process with the formation of intermediates pppApA or ppApA at pH 8.5 (50). observations were made in MsDisA synthetic reactions where c-di-AMP was produced via two intermediates, ppApA and pApA at pH 7.5. However, when we performed the enzyme assay at pH 9.4, we did not find any intermediate formation and c-di-AMP was produced rapidly. Our repetitive observation of high c-di-AMP synthetic rate at pH 9.4 made us to estimate the MsDisA promoter activity and we found that promoter activity is enhanced at alkaline pH. Hence, we clearly showed that at alkaline condition (pH 9.4), c-di-AMP is rapidly synthesized at high rate without any intermediate formation and at normal conditions (pH 7.5), it is synthesized slowly through the formation of two intermediates.

MsPDE is a homolog to the *M. tuberculosis* PDE (Rv2837c), consisting of two adjacent DHH and DHHA1 domains. In this type of PDE, c-di-AMP is degraded to AMP molecule via a pApA intermediate formation (26,32). Other PDEs, such as GDP in *B. subtilis* with an HD domain hydrolyzes c-di-AMP to pApA molecules (1). The reason for this difference is still unclear (1,28). Tang *et al.* 2015 (26) reported the formation of both pApA and AMP in *M. smegmatis*. However, we found only AMP peak in MsPDE catalyzed c-di-AMP hydrolysis at pH 7.5, whereas both pApA and AMP peaks were observed at pH 9.4. The rate of reaction is much slower at pH 9.4 when compared to that of the hydrolysis reaction at pH 7.5. Hence, we are

stating here that the rate of c-di-AMP hydrolysis is slower at alkaline condition than at normal condition.

Upon comparing the results of synthesis and hydrolysis reactions at different pH (7.5 and 9.4) by MsDisA and MsPDE, we are inclined to hypothesize that in *M. smegmatis,* during alkaline stress condition (pH 9.4) c-di-AMP is required at high concentration for the mycobacteria to withstand the stress and that is the reason for the synthesis at much higher rate and the hydrolysis at a slower rate at alkaline condition. In normal condition (pH 7.5), low level of c-di-AMP is good enough for the cells growth and hence the rate of synthesis is slow with the rapid hydrolysis.

The previous study that identified MsDisA (25) showed that in *M. smegmatis,* c-di-AMP is regulated by RadA, which directly interacts with MsDisA and acts as an antagonist for c-di-AMP synthesis. This kind of DisA and RadA interaction is conserved in bacteria. Zang et al., 2013 identified a c-di-AMP receptor DarR, which acts as a repressor of fatty acid synthesis genes in *M. smegmatis.* Another target of DarR is the cold shock CspA family protein which regulates low temperature stress response in *M. smegmatis* (17). In *M. tuberculosis,* DarR was shown to bind to c-di-AMP and stimulate the DNA binding (1, 17). These studies revealed the regulatory mechanism of c-di-AMP with respect to only MsDisA, whereas the present study speaks about the c-di-AMP homeostasis established by the balanced action of MsDisA and MsPDE during normal and alkaline stress conditions.

We noticed that the higher substrate concentration (ATP) inhibits the product (c-di-AMP) formation rate. Substrate-induced inhibition of MsDisA is interesting and directly links the critical balance of the second messenger as a function of cell growth. This is a typical case for cellular homeostasis of the second messenger. It should be noted that the inhibition by substrate was observed at all pH, albeit to a different extent. It was observed earlier that during c-di-GMP synthesis in *Pseudomonas aeruginosa,* di-guanylate cyclase (DGC) is regulated by an allosteric binding site for c-di-GMP, resulting in non-competitive product inhibition (51). Similar enzyme inhibition was also reported in Rv3586 (MtbDisA), where the diadenylate cyclase activity was negatively regulated by ATP or ADP (50). The MsDisA kinetic data also suggest that the cellular ATP pool may play an essential role in regulating the c-di-AMP concentration in cells. We presume that the higher ATP concentration during the exponential growth phase downregulates the c-di-AMP synthesis rate by allosterically inhibiting the enzyme activity, whereas in the

stationary growth phase lower ATP pool may induce a higher c-di-AMP synthesis. These kinetic experiments also provide valuable hints regarding cellular c-di-AMP concentration during bacterial growth phases and in varying physiological conditions. For example, in *S. aureus*, the c-di-AMP production increases during the late growth phase than during the log phase, and the c-di-AMP concentration is responsive to environmental stresses (52). The MsPDE kinetic data also follow the substrate inhibition model, and allosteric regulation was noticed for the c-di-AMP hydrolysis. However, the rate of c-di-AMP hydrolysis is higher at pH 7.5 than at pH 9.4 in vitro (**Fig. 7**).

We observed that the Cryo-EM structure of MsDisA is different from the *T. maritima* DisA. Active sites of *T. maritima* octamer were in closed conformation with D4 symmetry whereas MsDisA showed open conformation at the active site. We believed that this kind of open complex formation is necessary to accommodate ATP and hence the two monomers (Fig. 5C) are spaced out by 20 Å distance. As domain-3 of DisA is responsible for the DNA binding, and *T. maritima* DisA binds to DNA (13), we examined the DNA binding property of MsDisA protein by performing electrophoresis mobility shift assay with the synthetic Holliday junction DNA and double stranded DNA as used by Witte, Hartung et al. 2008 (13). We observed that the MsDisA protein did not show any binding to the Holliday junction or the double stranded DNA (Data not shown). Further analysis is required to understand the role of the C-terminal domain and if this is involved in binding to other molecules. This also prompted us to study the function of the individual domains the MsDisA.

The results as shown in Fig. 7 signify the importance of the N-terminal domain in the oligomerization and activity of the MsDisA. The putative C-terminal DNA binding domain possesses tetrameric symmetry (13), but N-terminal deleted mutant $MsDisA_{132\text{-}372}$ was inactive in c-di-AMP synthesis and did not form tetramers. We propose that the octamerization of the MsDisA occurs via the N-N terminal interaction. The involvement of domain-2 in oligomerization or during c-di-AMP synthesis is still unclear. It has been stated earlier that the deletion of the C-terminal domain makes the *M. tuberculosis* Rv3586 (DacA) a tetramer (32), while deletion of the N-terminal domain appeared as a dimer. Our biochemical data of the MsDisA mutants differ from the earlier observation regarding *M. tuberculosis* Rv3586 (DacA) (32). It, however, supports the crystal data of *T. maritima* DisA (PDB ID: 3C1Z) (13). Our study also emphasized the molecular assembly and symmetry of the protein, which are maintained

through the N-terminal domain-1 tetramerization. Furthermore, we infer that two MsDisA tetramers produce an octameric core (via N-terminal domain-1), and the interface of the N-N terminal tetramer acts as a substrate-binding region.

Since the N-terminal domain variant alone makes the necessary structure and function, we studied the active site residues of MsDisA and substrate specificity. It appears that MsDisA is unable to hydrolyze AMPCPP or AMPPCP suggesting direct participation of β-γ phosphate of ATP at the active site of the enzyme and ATP is the best substrate for MsDisA (Fig. S5 A and B). Stringent response factor (p)ppGpp acts as a competitive inhibitor of PDE activity of GdpP (53) and pgpH (54). However, we observed a contrary result to the observation made earlier (52), p(ppGpp) does not significantly affect the hydrolysis rate of c-di-AMP in *M. smegmatis*m *in vitro* (Fig. S5 C and D).

The research on c-di-AMP signaling is very active and under expansion due to its presence in plentiful microorganisms and the multiple phenotypes associated with the essential physiological functions. In addition, changes in c-di-AMP homeostasis affecting virulence and overall fitness of bacteria, especially pathogens such as *Mycobacterium tuberculosis* (where DisA is the only DAC which is an attractive target for further research to find a new direction of therapy; by controlling the c-di-AMP mediated signaling and by using its immunemodulatory properties (55). In this study we further expanded the mechanism of c-di-AMP regulatory mechanism and assigned one more type of stress response in the model organism *M. smegmatis*. However, the aspects of c-di-AMP regulation via (p)ppGpp and DNA binding properties of DisA in this organism is yet to be elucidated further to understand the unusual properties of MsDisA and MsPDE. Further studies in determining the structure of nucleotide bound MsDisA with ATP in particular to verify the structural changes observed here by CD spectroscopy and negative stain TEM is of significant interest.

Experimental procedures

Bacterial Strains and Growth condition

*M. smegmatis*mc^{2}155 and *Escherichia coli* strains used in this study are mentioned in Table S1. *M. smegmatis*mc^{2}155 strain was grown in MB7H9 medium (Difco) or MB7H9 medium solidified with 1.5% (w/v) agar with additional 2% glucose (vol/vol) and 0.05% Tween

80 (56). *E. coli* strains DH5α or BL21 (DE3) were grown in Luria-Bertani (LB) medium or in LB medium containing 1.5% (w/v) agar (57). Different antibiotics were used as required at the following concentrations: kanamycin (35 µg/ml) or ampicillin (100 µg/ml) for the respective *E. coli* strains.

Cloning and purification of DisA and PDE protein

To purify MsDisA as a C-terminally histidine-tagged protein, a DNA fragment (carrying *disA* gene / MSMEG_6080 / 1119 bp) was prepared using primers DisA1 and DisA2 (Table S2) and the *M. smegmatis mc^{2}155* genomic DNA as a template. The resulting PCR fragment was digested with *Nco*I and NotI, then ligated into the predigested pET28a plasmid. The pET28a plasmid carrying *disA* gene was transformed into *E. coli* DH5α cell. The clone was confirmed by DNA sequencing (Sigma). A similar approach was taken to clone MsPDE. A gene MSMEG_2630 (1023 bp) was amplified and cloned as stated earlier. Primer details are mentioned in Table S2.

MsDisA (372 aa) and MsPDE (340 aa) proteins were purified using a standard Ni-NTA column chromatography as demonstrated before (56,58). Briefly, *E. coli* BL21(DE3) cells containing plasmids for *disA* and *pde* were inoculated to LB medium respectively (supplemented with 35 µg/ml of kanamycin), followed by their growth overnight at 37^{0}C. Secondary cultures were prepared by taking 1% of the primary culture and grown at 37^{0}C with shaking till the OD_{600} reached at ~0.6. The cultures were then induced with 1mM isopropyl β-D-thiogalactopyranoside (IPTG) for 3hrs at 37^{0}C. The cultures were harvested by centrifugation at 6000rpm. The cells were then resuspended in lysis buffer (50 mM Tris-Cl; pH 7.9, 300 mM NaCl and 1mM phenyl-methylsulfonyl fluoride (PMSF) and lysed using probe sonication. The lysate was centrifuged at 14,000 r.p.m. to remove the cell debris. Then the supernatant was loaded onto a Ni-NTA column, allowed recombinant proteins to bind to the Ni-NTA beads, and then washed with 100 column volumes of wash buffer containing 40 mM imidazole. Finally, MsDisA and MsPDE proteins were eluted with the help of elution buffer containing 50 mM Tris-Cl; pH 7.9, 300 mM NaCl, and 300 mM imidazole. Different fractions collected during protein purification were analyzed by 10% SDS-PAGE. The eluted proteins were dialyzed against Tris-Cl buffer at pH 7.5, 300mM NaCl/KCl for 12−16hrs at 4°C or injected and purified on SEC (size exclusion chromatography)

column Superose 12 10/300 (GE Health care) against a buffer containing 50 mM Tris-Cl (pH 7.9) and 300 mM NaCl, and stored at -80°C for future use.

Cloning and purification of domain and point mutant proteins

The MsDisA single point mutants, D84A, D84E, H118A and H137A were generated by using MsDisA plasmid as a template. The primers for mutations are listed in Table S2. Site-directed mutagenesis (SDM) of Asp84, His118 and H137 residues was performed by a standard procedure (59). The PCR products were transformed into *E. coli* DH5α and a plasmid containing the mutation were confirmed by sequencing. The plasmids were transformed into *E. coli* BL21 (DE3) cells, and proteins were purified as described above.

Based on MsDisA cryo-EM structure, we defined and marked the domain boundaries and verified using the swiss-model program (https://swissmodel.expasy.org/interactive). To clone and express the respective domains of MsDisA proteins, DNA fragments (for specific MsDisA domain) were generated by PCR-amplification from *M. smegmatis* genomic using primers disA1-158A1/ disA1-158A2 (only N-Terminal domain-1), disA1-316A1/ disA1-316A2 (domain 1 and 2) and disA132-372A1/ disA132-372A2 (domain 2 and 3), respectively (Table-2). The amplicons for disA1-158aa, disA1-316aa and disA132-372aa, were digested with NcoI/NotI and cloned into the plasmid pET28a predigested with the same set of enzymes. The resulting plasmids pETdisA$_{1\text{-}158}$, pETdisA$_{1\text{-}316}$, and pETdisA$_{132\text{-}372}$ were transformed into *E. coli* BL21 (DE3) to express and purify as MsDisA mutant proteins. The protein purification was performed as described earlier with some modifications. Briefly, *the E. coli* BL21 (DE3) cells containing different plasmids 1-158 and 1-316 were grown in LB-broth to an OD_{600} at ~0.6, and the cultures were induced with 1mM IPTG, 3hrs at 37°C, and then harvested at 6,000 rpm and stored at -20° C for further use. For pETdisA$_{132\text{-}372,}$ *E. coli* BL21 containing plasmids were grown until OD reaches 0.6 at 37°C, cells were transferred to 18°C for 16h and induced with 0.1mM IPTG. Purification steps of the mutant proteins were followed as the protocol described for wild-type MsDisA protein.

Size exclusion chromatography-Multi Angle Light Scattering (SEC-MALS) and Gel filtration chromatography of the proteins

SEC-MALS experiment was performed to estimate the molecular mass and oligomerization of the purified proteins (MsDisA, MsPDE, and other mutant proteins) with a standard procedure. Briefly, a superdex 200 10/300 GL column (GE Health care) was equilibrated with 50 mM Tris-Cl buffer at pH 7.9 and 300 mM NaCl/KCl. 0.5 mg/ml of purified proteins were injected into the column separately, and the flow rate was fixed at 0.5 ml/min. To determine the molecular mass of the proteins, triple angle MALS detector (mini DawnTreos, Wyatt Technology), refractive index detector and UV detectors were used. Data analysis was finally done with the help of ASTRA software.

Activity assay of MsDisA, MsPDE and mutant proteins

The enzymatic assay of MsDisA, MsPDE and other mutant proteins was adapted from the protocol described with modifications (58,60,61). The assays were mainly aimed to study the synthesis and hydrolysis of c-di-AMP by MsDisA, MsPDE, and other mutant proteins. Briefly, to follow c-di-AMP synthesis by MsDisA and by other mutant proteins, samples were desalted in different buffer compositions (Buffer 1- 50 mM MES pH 5.4, 300 mM NaCl/KCl; Buffer 2- 50 mM Tris pH 7.5, 300 mM NaCl/KCl; and Buffer 3- 50 mM Tris pH 9.4, 300 mM NaCl/KCl). MsDisA protein (1µM) was incubated with 0.5 mM ATP and 5mM $MgCl_2$ at 37°C. The reactions were monitored for c-di-AMP synthesis, and reactions were stopped by adding EDTA (10mM), followed by centrifugation at 12000 r.p.m. for 30 min at 4°C. The MsPDE (0.25µM) protein was incubated with 0.5 mM c-di-AMP and 5mM $MgCl_2$ to study the hydrolase activity of MsPDE. Reactions were followed for 1 to 10 minutes, stopped by adding EDTA (10mM), and then centrifuged. Supernatants from the reaction samples were collected and subjected to HPLC analysis or stored at -20°C for further use. We performed the activity assay separately at different salt and pH levels to find the optimum pH and salt concentration of MsDisA and MsPDE activity. All the reactions were carried out following the same protocol as stated in the earlier section.

To assay substrate specificity, MsDisA protein was incubated with different substrates like ATP, ADP, AMPCPP, and AMPPCP and MsPDE reactions were performed with c-di-AMP c-di-GMP, cAMP, cGMP as substrates. The MsDisA assays were also conducted in the presence of different nucleotides ((p)ppGpp, GTP, GDP, PPi, and Pi) along with ATP. MsPDE assays

were also executed with c-di-GMP, (p)ppGpp, along with c-di-AMP. The assays were performed as a standard protocol described above, and the reaction products were analyzed by HPLC.

HPLC analysis

The synthesis of c-di-AMP by MsDisA or the hydrolysis of c-di-AMP by MsPDE proteins in different activity reactions were detected by HPLC analysis of the samples using a predefined protocol (58,62). A reverse phase C-18 column (4.6 x 150 mm, Agilent Eclipse XDB-C-18) was used to separate the reaction mixture containing nucleotides by an HPLC using buffer A (100 mM KH_2PO_4, 4 mM tetrabutylammonium hydrogen sulfate, pH 5.9) and buffer B (75 % (v/v) buffer A with 25 % (v/v) Methanol) (Agilent 1200). A different concentration gradient of c-di-AMP and AMP were used to prepare a standard curve for c-di-AMP and AMP. Area under the curve (AUC) values in the HPLC for each concentration of c-di-AMP was plotted against respective c-di-AMP concentration to prepare a c-di-AMP standard curve. Similarly, a standard curve for AMP was also produced from the AUC values of different AMP concentrations. The product formation from different activity assays of MsDisA, MsPDE or the mutant proteins was calculated from the standard curve. Each sample peak area was determined independently three times.

Enzyme kinetics

The enzyme activity of the MsDisA and MsPDE proteins were measured with varying substrate concentrations. MsDisA activity assay was performed for 4h with variable ATP concentration and different c-di-AMP concentrations were taken for MsPDE assay, where reactions were followed for 10 min. The reactions were performed using a standard protocol described earlier in the activity section (58). The reactions were stopped with the addition of EDTA (10mM) and followed by centrifugation of the samples at 12000 rpm at 4°C for 30 min. Samples were collected and subjected to HPLC analysis. The amount of c-di-AMP synthesized by the MsDisA production was calculated from the standard c-di-AMP curve at different concentrations. Similarly, the amount to AMP production was calculated from an AMP standard curve of varying concentrations. The kinetic parameters like K_m, K_i, and V_{max} were determined from the substrate inhibition model of enzyme kinetics (63) using GraphPad Prism (version 5.02).

$$Y=V_{max}*X/(K_m + X*(1+X/K_i) \qquad \text{Equation-1}$$

Vmax is the maximum enzyme velocity, expressed in the same units as the Y-axis. Km is the Michaelis-Menten constant, expressed in the same units as the X-axis. Ki is the dissociation constant for substrate binding so that two substrates can bind to an enzyme. It is expressed in the same units as X.

CD spectroscopic analysis

The secondary structural elements of MsDisA, MsPDE and other mutant proteins were determined from their far-UV CD spectra (200-260 nm). The CD spectra of these proteins were recorded at room temperature by a standard procedure using a JASCO J815 spectropolarimeter (56). The buffer values were subtracted from the corresponding spectra of protein samples. To determine the substrate-induced structural alteration of the MsDisA, MsPDE proteins, far-UV CD spectra of the MsDisA+ATP, and MsPDE+c-di-AMP complex were recorded. For MsDisA+ATP, ATP was incubated with MsDisA for 30min before the experiment.

Mass- spectroscopy and LC-MS analysis

A MALDI-TOF instrument was used to determine the molecular masses of the proteins and nucleotide molecules according to the manufacture's protocol (BurkerDaltonics, Germany). In-gel tryptic digestion was performed to confirm the MsDisA, MsPDE proteins and their domain variants by a standard protocol with some modification (64,65). The HPLC eluted fractions from the MsDisA and MsPDE reactions were analyzed by the LC-MS method (BurkerDaltonics, Germany)(56). MS-MS analysis (Negative or positive ion mode) of eluted molecular masses were performed to verify the presence of c-di-AMP and AMP. LC-MS and MSMS analysis were carried out by a standard protocol and the HPLC gradient composition was used as reported before (58).

Transmission electron microscopy (TEM) analysis of the proteins

FPLC purified MsDisA, MsDisAD84A, MsDisAH118A and the domain mutant proteins ($MsDisA_{1-158}$, $MsDisA_{1-316}$, and $MsDisA_{132-372}$) proteins were used for TEM grid preparation. The procedure for TEM grid preparation was described earlier in Ohi et al, 2004 (66). Briefly, carbon-coated copper grids (CF300-CU, Electron Microscopy Sciences) were glow discharged at 20mA for 90sec. Wild type MsDisA protein (0.05mg/mL) were applied (3.5µl) to the grid and let

it stand for 2 minutes at room temparature, followed by removal of the excess buffer using filter paper and then stained with 0.5 % of uranyl formate solution, then allowed to air dry. Grids were imaged with a Tecnai-T12 electron microscope operated with 120 kV at room temperature. Images were collected at a pixel of 2.54 Å/pixel on the specimen level on a side-mounted Olympus VELETA (2Kx2K) CCD camera. Protein particles were manually picked and extracted with box size of 160 Å from the raw micrographs using e2boxer.py. The two-dimensional reference-free classification of the extracted particles was performed using e2projectmanager.py (EMAN2.1 software) (67).

Cloning of putative MsDisA and MsPDE promoter regions

The putative promoter regions of MsDisA and MsPDE genes were cloned in a promoter-less vector pMN406, a promoter-less mycobacterium specific eGFP reporter vector. The pMN406 vector is a generous gift from Prof. Parthasarathi Ajithkumar (MCB, IISc-Bangalore) (68). The upstream regions of the *disA* gene (2400 bp) were PCR amplified using primers up-disA 2400F/up-disA 2400R. The amplicons were digested with XbaI and PacI enzymes and cloned upstream to the eGFP gene in the disApMN406 vector predigested with the same set of enzymes. The resulting recombinant plasmid-pMN2400, therefore, had the eGFP reporter gene just downstream of the MsDisA promoter. Similarly, the upstream region (1100bp) region of the *pde* gene was amplified and cloned using Xba1 and Sph1 enzymes (pdepMN1100). As a positive control, the hsp-60 promoter region was also cloned into the pMN406 vector. The recombinants plasmids were electroporated in *M. smegmatis mc*^{2} 155 competent cells and screened on MB7H9 agar plates (supplemented with 2% glucose) containing hygromycin (50 µg/ml). The *M. smegmatis* strains containing different promoter fragments were grown in MB7H9 medium supplemented with the required antibiotic. The strain also contains native promoters for *disA* and *pde* genes. However, their expression levels will be much less compared to that of vectors. As the readout is GFP, one is looking at the response of the vector alone.

Promoter induction assay

Our main objective was to measure the promoter induction of MsDisA and MsPDE in different conditions like pH and osmotic stress to follow the c-di-AMP homeostasis in the mycobacterial cell. To quantify the eGFP expression, *M. smegmatis* cells carrying the pMN406

(empty vector), disApMN2400, pdepMN1100, pMN-HSP plasmids were grown in MB7H9 broth supplemented with 2% glucose, 0.05% Tween 80 (v/v)and hygromycin (50 µg/ml). We have altered the pH (pH 5.4, 7.5, and 9.4) and the osmotic balance (0.5M NaCl/KCl) of the medium and the bacterial cells were then allowed to grow in these stress conditions. We also grew the cells under carbohydrate starving conditions (0.2% glucose used with MB7H9 broth). The growth kinetics of the *M. smegmatis* under different pH, salt, and glucose stress was also assayed. The bacterial cultures were harvested, and eGFP expression was measured using a fluorimeter (Jasco FP-6300) under different pH and salt stress. The harvested cultures (10 ml) were resuspended in 1 ml of buffer (50mM Tris pH 7.9 and 100mM NaCl) and sonicated, followed by centrifugation to obtain total protein content from the cells. Isolated total protein was normalized to 0.5mg/ml for all the samples. Further, eGFP expression was estimated from the fluorescence spectra of protein samples, measured between 480nm -600nm. The emission maxima (λ_{max}) values (at 509 nm) were then plotted against the growth time of the bacterial cells to study the promoter induction under different stress.

Binding affinity studies by Microscale Thermophoresis (MST)

For binding affinity measurement of MsDisA with ATP, MST was performed where the protein was labelled with Monolith Protein labelling kit RED-NHS. Fluorescent labelled MsDisA protein was mixed with ATP, ranging from 5mM to 153nM in ten-fold dilution concentrations. Samples were loaded on MST Premium Coated Monolith™ NT.115 capillaries, and measurements were done using Monolith NT.115pico. Further data analysis was done using Monolith Affinity Analysis software (version 2.3).

Grid preparation and CryoEM data collection

Purified MsDisA protein (50 mM Tris buffer pH 7.9 and 300mM NaCl) was applied to (3.0 µl of 0.1 mg/ml) glow discharged Quantifoil Cu 2.0/2.0, 300 mesh grids covered with a thin layer of home-made carbon using Thermo Fisher Scientific Vitrobot Mark IV. Grids were further incubated for 12s at > 95% relative humidity and blotted for 3.5 s. Immediately after blotting, the grids were plunge-frozen in liquid ethane.

The dataset was collected on a Titan Krios G3 transmission electron microscope equipped with a FEG at 300 kV with the automated data collection software EPU (Thermo Fisher Scientific) at

the National Cryo-EM facility, NCBS, Bangalore. Images of the MsDisA were collected with a Falcon III detector operating in counting mode at a nominal magnification of 75000× and a calibrated pixel size of 1.07 Å. Table S3 contains the details on defocus range, total electron dose, exposure time and frame number.

Data processing and model building

A total of 720 cryo-EM movie frames were motion-corrected by an algorithm inbuilt in Relion 3.0 (69). CTF estimation was performed with GCTF (70) on the full-dose weighted motion-corrected. A total of 4,29,709 particles were automatically selected using the Relion 3.0. auto-picking. The particles were extracted with a box size of 320 pixels. The extracted particles were imported into cryoSPARC 3.0 (36). Three rounds of reference-free 2d classification was carried out with 240 Å particle diameter to remove bad particles. 120,000 particles were selected and ab initio initial model generation was performed without any symmetry. After three ab initio models were generated, classes 1 and 2 with a total of ~80K particles, which have the whole protein's density, were selected for NU-refinement. The resolution of the 3D map was estimated at FSC 0.143. The local resolution of the map was estimated with Resmap (71). For model building of MsdisA, the model was predicted by the SWISS-MODEL or the *M.tuberculosis* DisA predicted by AlphaFold (37,38). The monomer of the MsDisA protein was manually fit into the cryo-EM map using UCSF Chimera and further inspected manually using Coot (72). The map from Cryosparc had the wrong hand (as deduced from the fit with the model) and the handedness was corrected. It was difficult to interpret the C-terminal region (in particular) of the auto sharpened map of MsDisA, thus different maps including those that have been sharpened with different B-factors, the unsharpened combined map, the map from phenix.local_aniso_sharpen (two half-maps as input and with default parameters) and the map from LocSpiral (73) were used for model building. As the C-terminus of the protein showed flexibility and had lower resolution, the side chains have been modelled only in the N-terminal domain and the rest of the model has only the backbone. The model was refined using Phenix real space refinement (74,75). Depending on the input map file (sharpened or unsharpened), the CC_mask and the group ADP value varied. We used the unsharpened map for the refinement as the C-terminal region was not blurred by sharpening.

Structural modeling, docking and Statistical analysis

Structural model of MsDisA protein generated from Phenix and was used for the molecular docking analysis by the Schrödinger program (Schrödinger Release 2021-1: CombiGlide, Schrödinger, LLC, New York, NY, 2021). The c-di-AMP and ATP molecules were docked with the MsDisA model structure to find the interacting residues of the MsDisA protein. All experimental analyses were performed in three different biological replicates (n=3).

Data availability

The data generated and analyzed in this study are included within the manuscript and supplementary data. The cryoEM map and the coordinates have not been deposited yet.

Supplementary Infomation

A supporting information document is available.

Acknowledgements

We thank our previous lab member Anushya Petchiappan for her valuable suggestions for preparing this manuscript. pMN406-ΔP_{imyc} empty vector was a gift from P. Ajitkumar.We thank Somnath Dutta and Priyanka Garg for initial data collection of cryo-EM and help in data processing. We thank Sunita Prakash for help in the mass-spectroscopy data acquisition and analysis. We thank Prateek Raj for his help in molecular docking analysis.

Author contributions

SG, AM and DC hypothesized and designed this study. SG, AM and AG carried out the experiments. SG, AM, KRV, SK and DC participated in data interpretation and manuscript preparation. YL made the cryoEM grids and performed the data collection. SG and YL performed image processing. SG, YL and KRV performed model building and analyzed the MsDisA cryo-EM structure.

Funding information

SG acknowledges UGC, Govt. of India for his fellowship. AM acknowledges support from the "DBT-RA Program in Biotechnology & Life Sciences" for fellowship. DC, AM and SG thanks Indian Institute of Science (IISc) for providing laboratory facility. DC acknowledges J C Bose fellowship and Honorary Professorship funding this work. KRV acknowledges SERB, India for the Ramanujan Fellowship (RJN-094/2017), and the support of the Department of Atomic

Energy, Government of India, under Project Identification No. RTI4006. We acknowledge the Department of Biotechnology, which support the National CryoEM facility, Bangalore (DBT B-Life grant DBT/PR12422/MED/31/287/2014).

Conflict of Interest

The authors declare that they have no conflicts of interest with the contents of this article.

References

1. Yin, W., Cai, X., Ma, H., Zhu, L., Zhang, Y., Chou, S. H., Galperin, M. Y., and He, J. (2020) A decade of research on the second messenger c-di-AMP. *FEMS Microbiol Rev* **44**, 701-724
2. Stulke, J., and Kruger, L. (2020) Cyclic di-AMP Signaling in Bacteria. *Annu Rev Microbiol* **74**, 159-179
3. Petchiappan, A., Mahapa, A., and Chatterji, D. (2020) Cyclic Dinucleotide Signaling in Mycobacteria. in *Microbial Cyclic Di-Nucleotide Signaling*, Springer. pp 3-25
4. Aline Dias da, P., Nathalia Marins de, A., Gabriel Guarany de, A., Robson Francisco de, S., and Cristiane Rodrigues, G. (2020) The World of Cyclic Dinucleotides in Bacterial Behavior. *Molecules* **25**
5. Gupta, K. R., Baloni, P., Indi, S. S., and Chatterji, D. (2016) Regulation of growth, cell shape, cell division, and gene expression by second messengers (p) ppGpp and cyclic Di-GMP in Mycobacterium smegmatis. *Journal of bacteriology* **198**, 1414-1422
6. Hauryliuk, V., Atkinson, G. C., Murakami, K. S., Tenson, T., and Gerdes, K. (2015) Recent functional insights into the role of (p) ppGpp in bacterial physiology. *Nature Reviews Microbiology* **13**, 298-309
7. Gupta, K. R., Kasetty, S., and Chatterji, D. (2015) Novel functions of (p)ppGpp and Cyclic di-GMP in mycobacterial physiology revealed by phenotype microarray analysis of wild-type and isogenic strains of Mycobacterium smegmatis. *Appl Environ Microbiol* **81**, 2571-2578
8. Romling, U., Galperin, M. Y., and Gomelsky, M. (2013) Cyclic di-GMP: the first 25 years of a universal bacterial second messenger. *Microbiol Mol Biol Rev* **77**, 1-52
9. Kalia, D., Merey, G., Nakayama, S., Zheng, Y., Zhou, J., Luo, Y., Guo, M., Roembke, B. T., and Sintim, H. O. (2013) Nucleotide, c-di-GMP, c-di-AMP, cGMP, cAMP, (p)ppGpp signaling in bacteria and implications in pathogenesis. *Chem Soc Rev* **42**, 305-341
10. Abdul-Sater, A. A., Tattoli, I., Jin, L., Grajkowski, A., Levi, A., Koller, B. H., Allen, I. C., Beaucage, S. L., Fitzgerald, K. A., Ting, J. P., Cambier, J. C., Girardin, S. E., and Schindler, C. (2013) Cyclic-di-GMP and cyclic-di-AMP activate the NLRP3 inflammasome. *EMBO Rep* **14**, 900-906
11. Petchiappan, A., Naik, S. Y., and Chatterji, D. (2020) RelZ-Mediated Stress Response in Mycobacterium smegmatis: pGpp Synthesis and Its Regulation. *J Bacteriol* **202**
12. Corrigan, R. M., and Gründling, A. (2013) Cyclic di-AMP: another second messenger enters the fray. *Nature Reviews Microbiology* **11**, 513-524

13. Witte, G., Hartung, S., Buttner, K., and Hopfner, K. P. (2008) Structural biochemistry of a bacterial checkpoint protein reveals diadenylate cyclase activity regulated by DNA recombination intermediates. *Mol Cell* **30**, 167-178
14. Fahmi, T., Port, G. C., and Cho, K. H. (2017) c-di-AMP: an essential molecule in the signaling pathways that regulate the viability and virulence of Gram-positive bacteria. *Genes* **8**, 197
15. Corrigan, R. M., Campeotto, I., Jeganathan, T., Roelofs, K. G., Lee, V. T., and Grundling, A. (2013) Systematic identification of conserved bacterial c-di-AMP receptor proteins. *Proc Natl Acad Sci U S A* **110**, 9084-9089
16. Zeden, M. S., Schuster, C. F., Bowman, L., Zhong, Q., Williams, H. D., and Gründling, A. (2018) Cyclic di-adenosine monophosphate (c-di-AMP) is required for osmotic regulation in Staphylococcus aureus but dispensable for viability in anaerobic conditions. *Journal of Biological Chemistry* **293**, 3180-3200
17. Zhang, L., Li, W., and He, Z.-G. (2013) DarR, a TetR-like transcriptional factor, is a cyclic di-AMP-responsive repressor in Mycobacterium smegmatis. *Journal of Biological Chemistry* **288**, 3085-3096
18. Woodward, J. J., Iavarone, A. T., and Portnoy, D. A. (2010) c-di-AMP secreted by intracellular Listeria monocytogenes activates a host type I interferon response. *Science* **328**, 1703-1705
19. Dey, B., Dey, R. J., Cheung, L. S., Pokkali, S., Guo, H., Lee, J. H., and Bishai, W. R. (2015) A bacterial cyclic dinucleotide activates the cytosolic surveillance pathway and mediates innate resistance to tuberculosis. *Nat Med* **21**, 401-406
20. Sauer, J.-D., Sotelo-Troha, K., Von Moltke, J., Monroe, K. M., Rae, C. S., Brubaker, S. W., Hyodo, M., Hayakawa, Y., Woodward, J. J., and Portnoy, D. A. (2011) The N-ethyl-N-nitrosourea-induced Goldenticket mouse mutant reveals an essential function of Sting in the in vivo interferon response to Listeria monocytogenes and cyclic dinucleotides. *Infection and immunity* **79**, 688-694
21. Burdette, D. L., Monroe, K. M., Sotelo-Troha, K., Iwig, J. S., Eckert, B., Hyodo, M., Hayakawa, Y., and Vance, R. E. (2011) STING is a direct innate immune sensor of cyclic di-GMP. *Nature* **478**, 515-518
22. Manzanillo, P. S., Shiloh, M. U., Portnoy, D. A., and Cox, J. S. (2012) Mycobacterium tuberculosis activates the DNA-dependent cytosolic surveillance pathway within macrophages. *Cell host & microbe* **11**, 469-480
23. Zhang, Z., Yuan, B., Bao, M., Lu, N., Kim, T., and Liu, Y. J. (2011) The helicase DDX41 senses intracellular DNA mediated by the adaptor STING in dendritic cells. *Nat Immunol* **12**, 959-965
24. Zhang, X., Shi, H., Wu, J., Zhang, X., Sun, L., Chen, C., and Chen, Z. J. (2013) Cyclic GMP-AMP containing mixed phosphodiester linkages is an endogenous high-affinity ligand for STING. *Molecular cell* **51**, 226-235
25. Zhang, L., and He, Z. G. (2013) Radiation-sensitive gene A (RadA) targets DisA, DNA integrity scanning protein A, to negatively affect cyclic Di-AMP synthesis activity in Mycobacterium smegmatis. *J Biol Chem* **288**, 22426-22436
26. Tang, Q., Luo, Y., Zheng, C., Yin, K., Ali, M. K., Li, X., and He, J. (2015) Functional analysis of a c-di-AMP-specific phosphodiesterase MsPDE from Mycobacterium smegmatis. *International journal of biological sciences* **11**, 813

27. He, Q., Wang, F., Liu, S., Zhu, D., Cong, H., Gao, F., Li, B., Wang, H., Lin, Z., and Liao, J. (2016) Structural and biochemical insight into the mechanism of Rv2837c from Mycobacterium tuberculosis as a c-di-NMP phosphodiesterase. *Journal of Biological Chemistry* **291**, 3668-3681
28. Commichau, F. M., Heidemann, J. L., Ficner, R., and Stülke, J. (2019) Making and Breaking of an Essential Poison: the Cyclases and Phosphodiesterases That Produce and Degrade the Essential Second Messenger Cyclic di-AMP in Bacteria. *Journal of bacteriology* **201**, e00462-00418
29. Whiteley, A. T., Pollock, A. J., and Portnoy, D. A. (2015) The PAMP c-di-AMP is essential for Listeria monocytogenes growth in rich but not minimal media due to a toxic increase in (p) ppGpp. *Cell host & microbe* **17**, 788-798
30. Yang, J., Bai, Y., Zhang, Y., Gabrielle, V. D., Jin, L., and Bai, G. (2014) Deletion of the cyclic di-AMP phosphodiesterase gene (cnpB) in Mycobacterium tuberculosis leads to reduced virulence in a mouse model of infection. *Mol Microbiol* **93**, 65-79
31. Manikandan, K., Sabareesh, V., Singh, N., Saigal, K., Mechold, U., and Sinha, K. M. (2014) Two-step synthesis and hydrolysis of cyclic di-AMP in Mycobacterium tuberculosis. *PloS one* **9**
32. Bai, Y., Yang, J., Zhou, X., Ding, X., Eisele, L. E., and Bai, G. (2012) Mycobacterium tuberculosis Rv3586 (DacA) is a diadenylate cyclase that converts ATP or ADP into c-di-AMP. *PloS one* **7**, e35206
33. Talley, K., and Alexov, E. (2010) On the pH-optimum of activity and stability of proteins. *Proteins: Structure, Function, and Bioinformatics* **78**, 2699-2706
34. Devaux, L., Sleiman, D., Mazzuoli, M.-V., Gominet, M., Lanotte, P., Trieu-Cuot, P., Kaminski, P.-A., and Firon, A. (2018) Cyclic di-AMP regulation of osmotic homeostasis is essential in Group B Streptococcus. *PLoS genetics* **14**, e1007342
35. Zivanov, J., Nakane, T., Forsberg, B. O., Kimanius, D., Hagen, W. J., Lindahl, E., and Scheres, S. H. (2018) New tools for automated high-resolution cryo-EM structure determination in RELION-3. *elife* **7**
36. Punjani, A., Rubinstein, J. L., Fleet, D. J., and Brubaker, M. A. (2017) cryoSPARC: algorithms for rapid unsupervised cryo-EM structure determination. *Nat Methods* **14**, 290-296
37. Waterhouse, A., Bertoni, M., Bienert, S., Studer, G., Tauriello, G., Gumienny, R., Heer, F. T., de Beer, T. A. P., Rempfer, C., Bordoli, L., Lepore, R., and Schwede, T. (2018) SWISS-MODEL: homology modelling of protein structures and complexes. *Nucleic Acids Res* **46**, W296-W303
38. Jumper, J., Evans, R., Pritzel, A., Green, T., Figurnov, M., Ronneberger, O., Tunyasuvunakool, K., Bates, R., Zidek, A., Potapenko, A., Bridgland, A., Meyer, C., Kohl, S. A. A., Ballard, A. J., Cowie, A., Romera-Paredes, B., Nikolov, S., Jain, R., Adler, J., Back, T., Petersen, S., Reiman, D., Clancy, E., Zielinski, M., Steinegger, M., Pacholska, M., Berghammer, T., Bodenstein, S., Silver, D., Vinyals, O., Senior, A. W., Kavukcuoglu, K., Kohli, P., and Hassabis, D. (2021) Highly accurate protein structure prediction with AlphaFold. *Nature* **596**, 583-589
39. Friesner, R. A., Banks, J. L., Murphy, R. B., Halgren, T. A., Klicic, J. J., Mainz, D. T., Repasky, M. P., Knoll, E. H., Shelley, M., and Perry, J. K. (2004) Glide: a new approach for rapid, accurate docking and scoring. 1. Method and assessment of docking accuracy. *Journal of medicinal chemistry* **47**, 1739-1749

40. Gibhardt, J., Hoffmann, G., Turdiev, A., Wang, M., Lee, V. T., and Commichau, F. M. (2019) c-di-AMP assists osmoadaptation by regulating the Listeria monocytogenes potassium transporters KimA and KtrCD. *J Biol Chem* **294**, 16020-16033
41. Kim, H., Youn, S. J., Kim, S. O., Ko, J., Lee, J. O., and Choi, B. S. (2015) Structural Studies of Potassium Transport Protein KtrA Regulator of Conductance of K+ (RCK) C Domain in Complex with Cyclic Diadenosine Monophosphate (c-di-AMP). *J Biol Chem* **290**, 16393-16402
42. Bowman, L., Zeden, M. S., Schuster, C. F., Kaever, V., and Gründling, A. (2016) New insights into the cyclic di-adenosine monophosphate (c-di-AMP) degradation pathway and the requirement of the cyclic dinucleotide for acid stress resistance in Staphylococcus aureus. *Journal of Biological Chemistry* **291**, 26970-26986
43. Gándara, C., and Alonso, J. C. (2015) DisA and c-di-AMP act at the intersection between DNA-damage response and stress homeostasis in exponentially growing Bacillus subtilis cells. *DNA repair* **27**, 1-8
44. Oppenheimer-Shaanan, Y., Wexselblatt, E., Katzhendler, J., Yavin, E., and Ben-Yehuda, S. (2011) c-di-AMP reports DNA integrity during sporulation in Bacillus subtilis. *EMBO Rep* **12**, 594-601
45. Pham, H. T., Shi, W., Xiang, Y., Foo, S. Y., Plan, M. R., Courtin, P., Chapot-Chartier, M. P., Smid, E. J., Liang, Z. X., Marcellin, E., and Turner, M. S. (2021) Cyclic di-AMP Oversight of Counter-Ion Osmolyte Pools Impacts Intrinsic Cefuroxime Resistance in Lactococcus lactis. *mBio* **12**
46. Rubin, B. E., Huynh, T. N., Welkie, D. G., Diamond, S., Simkovsky, R., Pierce, E. C., Taton, A., Lowe, L. C., Lee, J. J., Rifkin, S. A., Woodward, J. J., and Golden, S. S. (2018) High-throughput interaction screens illuminate the role of c-di-AMP in cyanobacterial nighttime survival. *PLoS Genet* **14**, e1007301
47. Peng, X., Zhang, Y., Bai, G., Zhou, X., and Wu, H. (2016) Cyclic di-AMP mediates biofilm formation. *Mol Microbiol* **99**, 945-959
48. Whiteley, A. T., Garelis, N. E., Peterson, B. N., Choi, P. H., Tong, L., Woodward, J. J., and Portnoy, D. A. (2017) c-di-AMP modulates Listeria monocytogenes central metabolism to regulate growth, antibiotic resistance and osmoregulation. *Mol Microbiol* **104**, 212-233
49. Dey, R. J., Dey, B., Zheng, Y., Cheung, L. S., Zhou, J., Sayre, D., Kumar, P., Guo, H., Lamichhane, G., Sintim, H. O., and Bishai, W. R. (2017) Inhibition of innate immune cytosolic surveillance by an M. tuberculosis phosphodiesterase. *Nat Chem Biol* **13**, 210-217
50. Manikandan, K., Sabareesh, V., Singh, N., Saigal, K., Mechold, U., and Sinha, K. M. (2014) Two-step synthesis and hydrolysis of cyclic di-AMP in Mycobacterium tuberculosis. *PloS one* **9**, e86096
51. Christen, B., Christen, M., Paul, R., Schmid, F., Folcher, M., Jenoe, P., Meuwly, M., and Jenal, U. (2006) Allosteric control of cyclic di-GMP signaling. *Journal of Biological Chemistry* **281**, 32015-32024
52. Corrigan, R. M., Bowman, L., Willis, A. R., Kaever, V., and Gründling, A. (2015) Cross-talk between two nucleotide-signaling pathways in Staphylococcus aureus. *Journal of Biological Chemistry* **290**, 5826-5839

53. Rao, F., See, R. Y., Zhang, D., Toh, D. C., Ji, Q., and Liang, Z.-X. (2010) YybT is a signaling protein that contains a cyclic dinucleotide phosphodiesterase domain and a GGDEF domain with ATPase activity. *Journal of Biological Chemistry* **285**, 473-482
54. Huynh, T. N., Luo, S., Pensinger, D., Sauer, J. D., Tong, L., and Woodward, J. J. (2015) An HD-domain phosphodiesterase mediates cooperative hydrolysis of c-di-AMP to affect bacterial growth and virulence. *Proc Natl Acad Sci U S A* **112**, E747-756
55. Libanova, R., Becker, P. D., and Guzmán, C. A. (2012) Cyclic di-nucleotides: new era for small molecules as adjuvants. *Microbial biotechnology* **5**, 168-176
56. Bharati, B. K., Mukherjee, R., and Chatterji, D. (2018) Substrate-induced domain movement in a bifunctional protein, DcpA, regulates cyclic di-GMP turnover: Functional implications of a highly conserved motif. *J Biol Chem* **293**, 14065-14079
57. Russell, D. W., and Sambrook, J. (2001) *Molecular cloning: a laboratory manual*, Cold Spring Harbor Laboratory Cold Spring Harbor, NY
58. Bharati, B. K., Sharma, I. M., Kasetty, S., Kumar, M., Mukherjee, R., and Chatterji, D. (2012) A full-length bifunctional protein involved in c-di-GMP turnover is required for long-term survival under nutrient starvation in Mycobacterium smegmatis. *Microbiology* **158**, 1415-1427
59. Krishnan, S., Petchiappan, A., Singh, A., Bhatt, A., and Chatterji, D. (2016) R-loop induced stress response by second (p)ppGpp synthetase in Mycobacterium smegmatis: functional and domain interdependence. *Mol Microbiol* **102**, 168-182
60. Christen, M., Christen, B., Folcher, M., Schauerte, A., and Jenal, U. (2005) Identification and characterization of a cyclic di-GMP-specific phosphodiesterase and its allosteric control by GTP. *Journal of Biological Chemistry* **280**, 30829-30837
61. Bai, Y., Yang, J., Zhou, X., Ding, X., Eisele, L. E., and Bai, G. (2012) Mycobacterium tuberculosis Rv3586 (DacA) is a diadenylate cyclase that converts ATP or ADP into c-di-AMP. *PloS one* **7**
62. Ryjenkov, D. A., Tarutina, M., Moskvin, O. V., and Gomelsky, M. (2005) Cyclic diguanylate is a ubiquitous signaling molecule in bacteria: insights into biochemistry of the GGDEF protein domain. *J Bacteriol* **187**, 1792-1798
63. Copeland, R. A. (2000) *Enzymes: a practical introduction to structure, mechanism, and data analysis*, John Wiley & Sons
64. Henzel, W. J., Watanabe, C., and Stults, J. T. (2003) Protein identification: the origins of peptide mass fingerprinting. *J Am Soc Mass Spectrom* **14**, 931-942
65. Suckau, D., Resemann, A., Schuerenberg, M., Hufnagel, P., Franzen, J., and Holle, A. (2003) A novel MALDI LIFT-TOF/TOF mass spectrometer for proteomics. *Anal Bioanal Chem* **376**, 952-965
66. Ohi, M., Li, Y., Cheng, Y., and Walz, T. (2004) Negative Staining and Image Classification - Powerful Tools in Modern Electron Microscopy. *Biol Proced Online* **6**, 23-34
67. Tang, G., Peng, L., Baldwin, P. R., Mann, D. S., Jiang, W., Rees, I., and Ludtke, S. J. (2007) EMAN2: an extensible image processing suite for electron microscopy. *J Struct Biol* **157**, 38-46
68. Roy, S., Narayana, Y., Narayanaswamy Balaji, K., and Ajitkumar, P. (2012) Highly fluorescent GFPm2+-based genome integration-proficient promoter probe vector to study Mycobacterium tuberculosis promoters in infected macrophages. *Microbial biotechnology* **5**, 98-105

69. Scheres, S. H. (2012) RELION: implementation of a Bayesian approach to cryo-EM structure determination. *J Struct Biol* **180**, 519-530
70. Zhang, K. (2016) Gctf: Real-time CTF determination and correction. *J Struct Biol* **193**, 1-12
71. Kucukelbir, A., Sigworth, F. J., and Tagare, H. D. (2014) Quantifying the local resolution of cryo-EM density maps. *Nat Methods* **11**, 63-65
72. Emsley, P., Lohkamp, B., Scott, W. G., and Cowtan, K. (2010) Features and development of Coot. *Acta Crystallogr D Biol Crystallogr* **66**, 486-501
73. Kaur, S., Gomez-Blanco, J., Khalifa, A. A. Z., Adinarayanan, S., Sanchez-Garcia, R., Wrapp, D., McLellan, J. S., Bui, K. H., and Vargas, J. (2021) Local computational methods to improve the interpretability and analysis of cryo-EM maps. *Nat Commun* **12**, 1240
74. Adams, P. D., Afonine, P. V., Bunkoczi, G., Chen, V. B., Davis, I. W., Echols, N., Headd, J. J., Hung, L. W., Kapral, G. J., Grosse-Kunstleve, R. W., McCoy, A. J., Moriarty, N. W., Oeffner, R., Read, R. J., Richardson, D. C., Richardson, J. S., Terwilliger, T. C., and Zwart, P. H. (2010) PHENIX: a comprehensive Python-based system for macromolecular structure solution. *Acta Crystallogr D Biol Crystallogr* **66**, 213-221
75. Afonine, P. V., Poon, B. K., Read, R. J., Sobolev, O. V., Terwilliger, T. C., Urzhumtsev, A., and Adams, P. D. (2018) Real-space refinement in PHENIX for cryo-EM and crystallography. *Acta Crystallogr D Struct Biol* **74**, 531-544

Tables

Table1: Enzyme kinetics of MsDisA protein at different pH of the buffer

MsDisA	**pH 5.4**	**pH 7.5**	**pH 9.4**
Vmax (mM/min)	0.15	0.21	1.44
Km (mM)	1.10	0.48	0.94
Ki (mM)	3.30	1.43	2.81

Table 2: Enzyme kinetic of MsPDE protein at different pH of the buffer

MsPDE	**pH 5.4**	**pH 7.5**	**pH 9.4**
Vmax (mM/min)	0.07	1.64	1.73
Km (mM)	0.31	0.37	0.85
Ki (mM)	0.94	1.12	2.55

Table 3: Binding parameters of MsDisA protein with ATP at different pH of the buffer.

Protein in 75mM NaCl and 50mM Tris/MES at diffrent pH	Ligand	K_d(µM)
MsDisA at pH 5.4	ATP	968
MsDisA at pH 7.5	ATP	2.4
MsDisA at pH 9.4	ATP	15

Figures

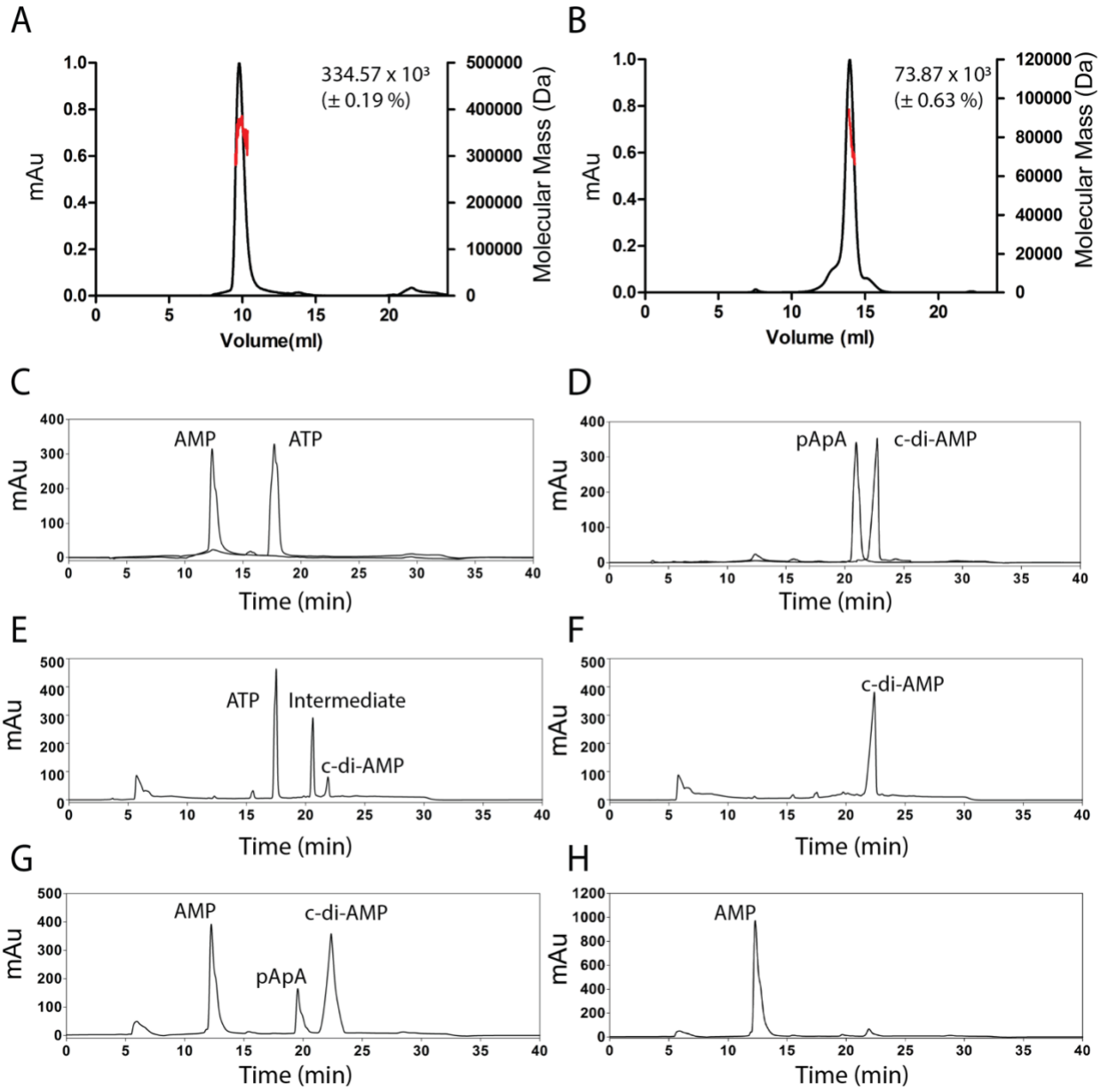

Fig. 1 - Biochemical analysis of the MsDisA and MsPDE proteins. (A) SEC-MALS profile of MsDisA (0.5 mg/mL) indicates octameric molecular mass of 334.5±0.19 kD. (B) SEC-MALS profile of MsPDE (0.5 mg/mL) indicates dimeric molecular mass of 73.8 ±0.63 kD . (C and D) HPLC profiles of commercial AMP, ATP, pApA and c-di-AMP molecules (250µM). The elution volume of the nucleotide are 12.2, 17.4, 20.3 and 23.7 mins, respectively. (E and F) Analysis of the MsDisA (1µM) with ATP (500µM) in reaction products at 50mM Tris-Cl, 75mM NaCl at pH 7.5 and pH 9.4 (4Hrs), respectively. HPLC profile (E) showed c-di-AMP synthetic

intermediates formation in the MsDisA reactions at pH 7.5. (G and H) Analysis of the MsPDE (0.25 µM) with c-di-AMP (500µM) in reaction products at 50mM Tris-Cl, 75mM NaCl at pH 9.4 and pH 7.5 (10min), respectively. HPLC profile (G) showed c-di-AMP hydrolysis intermediate in the MsPDE reactions at pH 9.4.

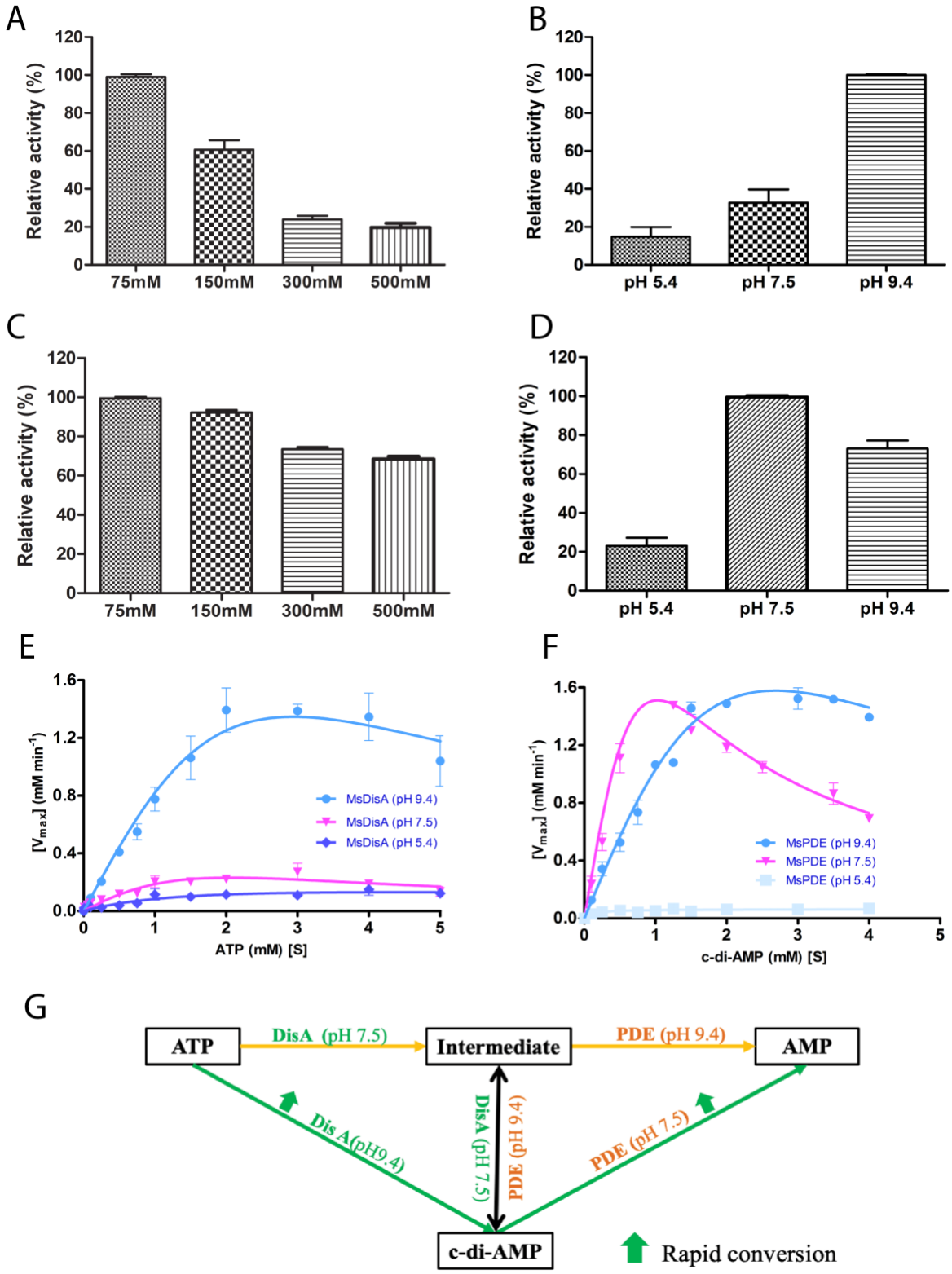

Fig. 2 - MsDisA and MsPDE activity at different conditions. (A) MsDisA activity at varying salt (75 to 500mM NaCl) at pH 9.4 for 4hrs. (B) MsDisA activity at varying pH (5.4 to 9.4) with

75 NaCl for 4hrs. (C) MsPDE at varying salt (75 to 500mM) at pH 7.5 in 10min. (D) MsPDE at varying pH (5.4 to 9.4), 75 NaCl for 10 min. (E) Steady-state enzyme kinetics plot for c-di-AMP synthesis in different conditions (pH 9.4, 7.5 and 5.4). (F) Steady-state enzyme kinetics plot for the c-di-AMP hydrolysis in different conditions (pH 9.4, 7.5 and 5.4). (G) Catalytic model of MsDisA and MsPDE under salt and pH stress *in vitro.** In MsDisA reactions complete conversion of ATP (500µM) to c-di-AMP in a given time is considered 100% relative activity (Ex- **Fig. 1F**). ** In MsPDE reactions complete conversion of c-di-AMP (500µM) to AMP in a given time is considered 100% relative activity (Ex- **Fig. 1H**).

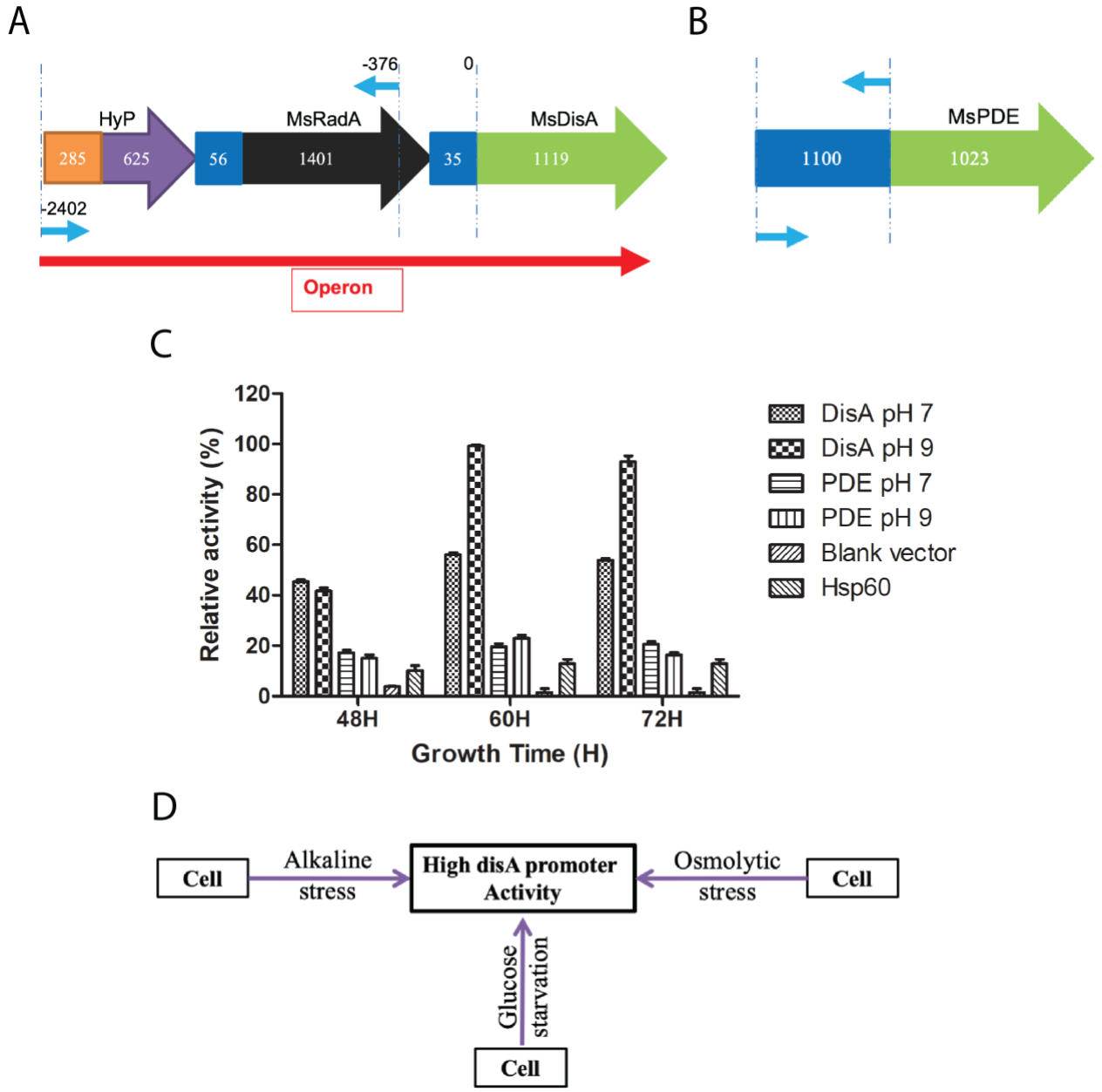

Fig. 3 - Promoter activity assay of the MsDisA and MsPDE gene: (A and B) Graphical representation of the *disA* and *pde* upstream gene elements. (C) MsDisA and MsPDE promoter activity assay under neutral (pH 7.5) and alkaline pH (pH 9.4) during mycobacterial growth. Hsp60 and blank vector were used as positive and negative control for the experiment, respectively. (D) Schematic representation of the MsDisA promoter activity under different conditions.

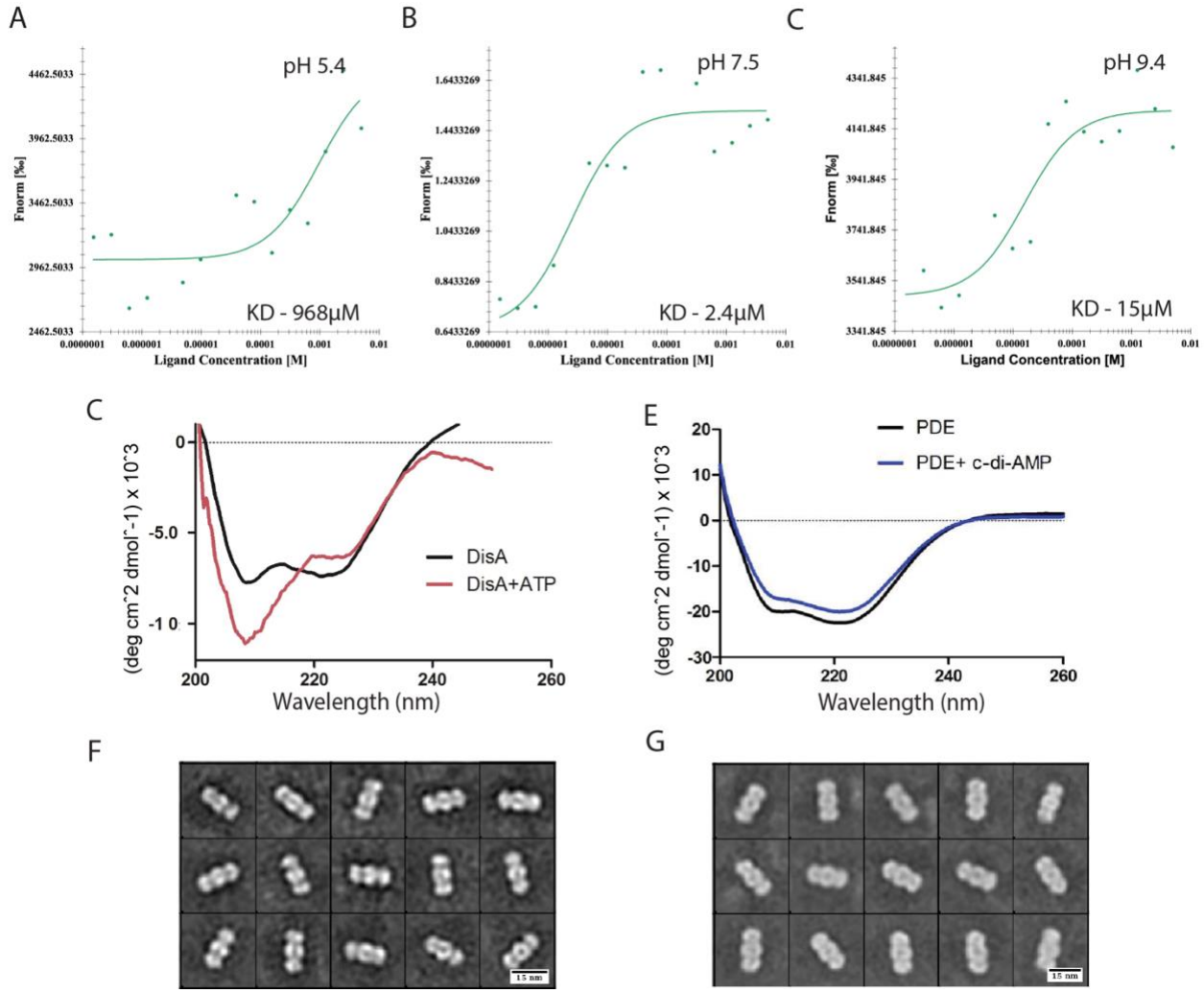

Fig. 4- Substrate induced structural alteration of the MsDisA and MsPDE proteins. (A-C) Binding affinity of MsDisA with ATP at varing pH by MST (A-pH 5.4, B- pH 7.5 and C-pH 9.4). Non-labelled ATP in the concetration range from 5mM to 153 nM were titrated with 20nM labelled MsDisA. K_d values are mentioned in the respective graphs at different pH. (D) Far-UV CD spectra of the MsDisA and MsDisA + ATP (500µM) complex. (E) Far-UV CD spectra of the MsPDE and MsPDE + c-di-AMP (500µM) complex. (F and G) TEM 2D class averages of the MsDisA (Pacticle length- 17.58 ±1.07 nm) and MsDisA + 500µM ATP complex (Particle length- 19.73 ±0.95 nm) (box size is 240 pixels).

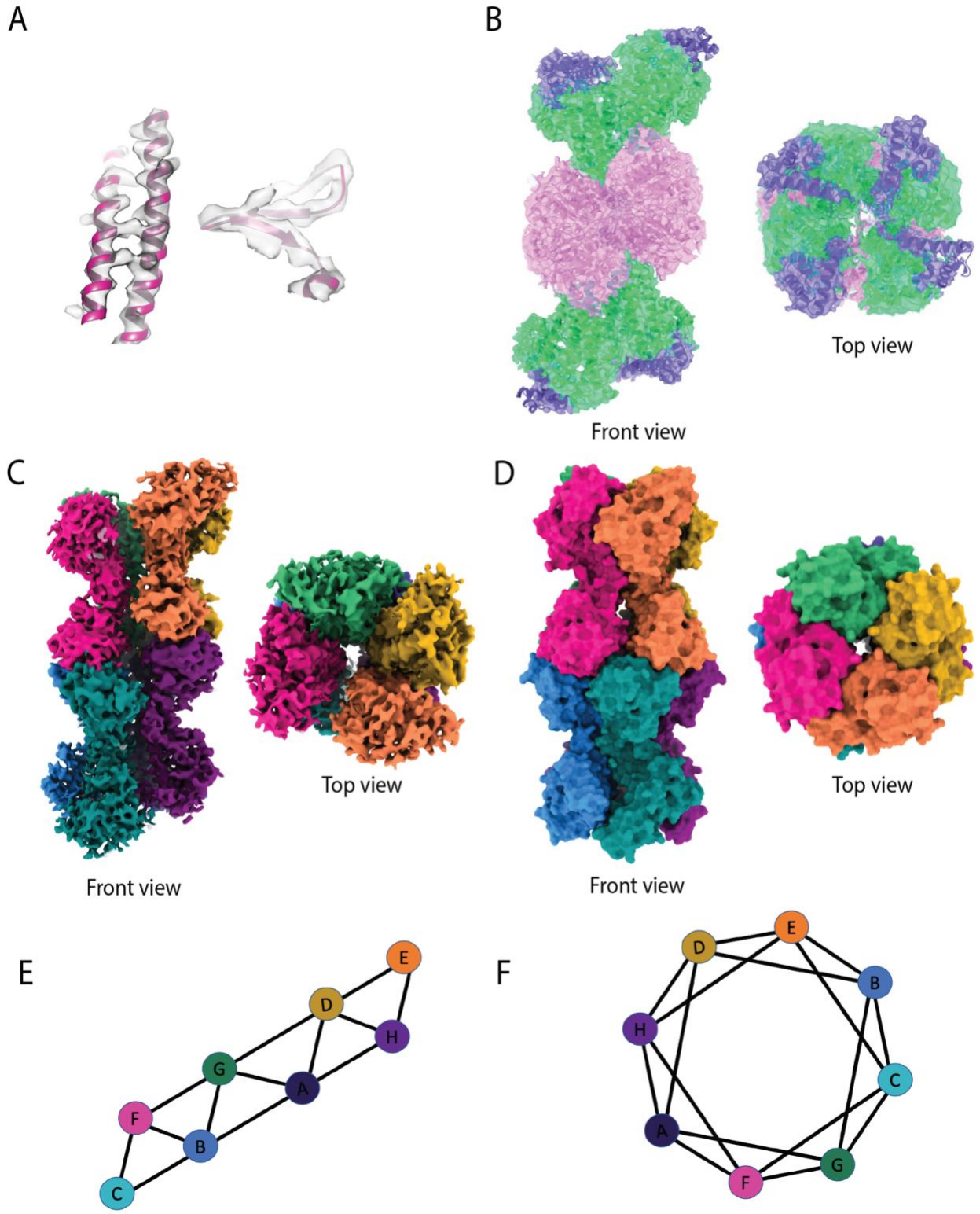

Fig. 5 - Structural investigation of MsDisA by Cryo-EM. (A) Representative secondary structural regions of the electron density map of MsDisA at ~3.8 Å resolution. (B) AlphaFold

model docked in the cryo-EM map with domain boundaries marked including front and top views. (C) Cryo-EM map of the MsDisA. Each monomer is represented with a different colour. (D) The surface model of *Tm*DisA (PDB-3C1Z), front and top views show D4 symmetry, whereas MsDisA shows deviation from D4 symmetry in solution, exhibiting an open confirmation as seen in Fig. 5C. (E and F) Interfaces tool in chimeraX showing MsDisA open structure. MsDisA map has eight monomeric chains having 13 contacts, whereas *Tm*DisA (PDB-3C1Z) has 16 connections among eight monomers.

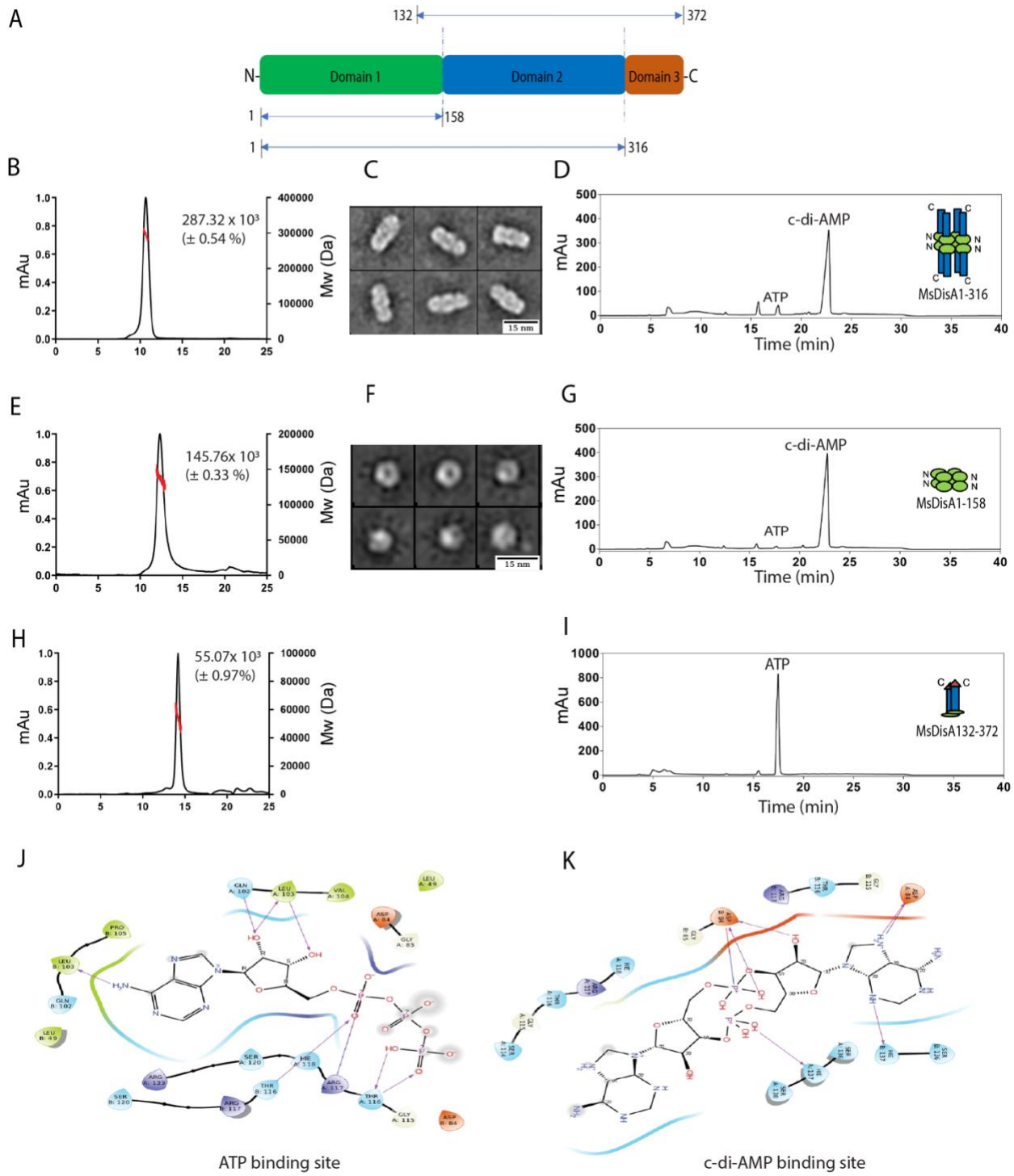

Fig. 6 - Analysis of the MsDisA domain mutants. (A) Domain architecture of monomeric MsDisA. (B) SEC-MALS profile of $MsDisA_{1-316}$ (0.5 mg/mL) indicates octameric molecular mass of 287.32 kDa. (C) TEM images of the $MsDisA_{1-316}$ (box size of 220 pixels, length- 15.77 ±0.78). (D) HPLC profile of the activity analysis of the $MsDisA_{1-316}$ along with oligomeric

model cartoon. (E) SEC-MALS profile of $MsDisA_{1-158}$ (0.5 mg/mL) indicates octameric molecular mass of 145.76 kDa. (F) TEM images of the $MsDisA_{1-158}$ (box size of 200 pixels, length- 10.72 ±2.49). (G) HPLC profile of the activity analysis of the $MsDisA_{1-158}$ with oligomeric model. (H) SEC-MALS profile of $MsDisA_{132-372}$ (0.5 mg/mL) indicates dimer molecular mass of 55.70 kDa. (I) HPLC profile of the activity analysis of the $MsDisA_{132-372}$ along with dimeric model. (J and K) Molecular docking analysis of MsDisA active site with ATP and c-di-AMP. The synthesis activity in each case was carried out as shown in fig. 1.

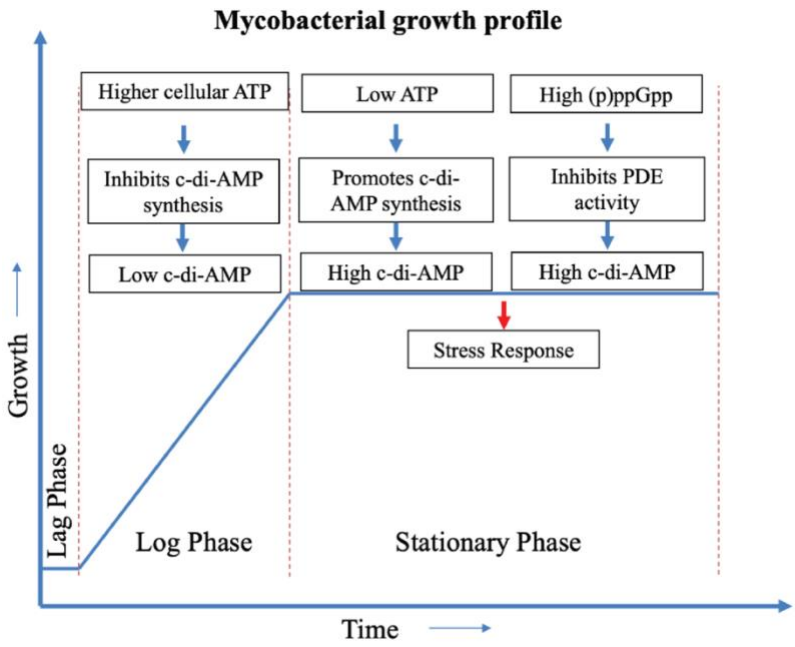

Fig. 7 – Schematic presentation of the MsDisA and MsPDE activity as a function of mycobacterial growth.

From this study we propose that during the log phase of mycobacterial growth, intracellular c-di-AMP concentration is down-regulated by the higher ATP level in the cell as shown by our kinetic studies (**Fig. 2E**). Whereas, at stationary phase of the mycobacterial growth (48-72hrs) the lower ATP pool and higher (p)ppGpp or c-di-GMP level up-regulate the c-di-AMP production as we noticed higher promoter activity at stationary phase (**Fig. 3C**).